Theory of cascade correlated emission from atom arrays

P. R. Berman and A. Kuzmich
Physics Department, University of Michigan, Ann Arbor, Michigan 48109-1040, USA

(Received 25 January 2024; accepted 29 April 2024; published 16 May 2024)

We present a theory of cascade emission from an array of N fixed, "three-level" atoms. The total angular momentum of the ground state of each atom is $J = 0$, that of the intermediate state is $J = 1$, and that of the upper state is $J = 0$. The atoms are prepared in a spatially phased superposition of their ground and upper states, collectively sharing a single excitation. We calculate the time-integrated, joint probability distribution for radiation to be emitted in a given direction with a given polarization on each transition and use this joint probability distribution to calculate the time-integrated intensity emitted on each transition. The dipole-dipole interaction between the atoms is taken into account. Analytic expressions are obtained for two atoms and the calculation is then extended formally to an ensemble of N atoms at arbitrary positions. As expected, the radiation emitted on the upper transition is unpolarized and isotropic. However, somewhat surprisingly, we find that for excitation by counterpropagating fields and for nearly equal ground to intermediate and intermediate to upper level transition frequencies, the radiation on the lower transition is also isotropic and unpolarized, provided the atoms are prepared in a fully symmetric state. We also establish conditions for which there can be a phase-matched enhancement of the joint probability density for specific directions of emissions on the upper and lower transitions.

DOI: 10.1103/PhysRevA.109.053714

I. INTRODUCTION

The realization of efficient quantum light-matter interfaces represents an important step in the development of scalable quantum communication networks [1,2]. In particular, coupling telecommunication-wavelength light to matter qubits is needed for optical-fiber implementations of such networks. This can be achieved by using hosts such as optical crystals [3], waveguides [4], or fibers [5] doped with erbium ions, which possess suitable telecommunication transitions from the ground state. Neutral atoms such as rubidium and cesium do not possess telecom transitions originating in the ground atomic state. However, cascade (ladder) level configurations exist with suitable C-band telecom transitions [6]. Using optical storage and retrieval pulses to drive these transitions, efficient and noiseless generation of telecom light has been realized [7] in a cold rubidium vapor and extended to entanglement of telecom-wavelength light with atomic qubits trapped in a state-insensitive optical lattice [8]. Recently, a broadband quantum memory for telecom light has been demonstrated using a ladder level scheme in a hot [9] rubidium vapor. Extending these approaches to Rydberg-array-based memories would allow one to incorporate neutral-atom quantum processors into distributed quantum networks. The same cascade level scheme in Rb or Cs has been used for entanglement generation between telecom and near-IR fields based on both ultracold [6] or hot [10] vapors. Memory-light entanglement can be subsequently created by either mapping the near-IR field into an atomic memory or by entanglement swapping with a Raman-type atom-field entangled state.

Given the scope of these applications, it is important to have first-principle calculations of cascade emission in which the magnetic state degeneracy is taken into account. In a recent article [11], we studied cascade emission from an ensemble of "three-level" atoms in the limit that the probability to have more than one excitation in the ensemble was negligible. Interactions between the atoms were included implicitly within the framework of an approximation made by Rehler and Eberly (RE) [12] in their study of superradiance. It was pointed out that, although the RE model provides good agreement with the exact solution, it can lead to some physical inconsistencies. For example, when applied to cascade decay, it can result in a prediction that the emission on the upper transition is anisotropic and polarized, whereas, in actuality, the radiation emitted on this transition is unpolarized and isotropic. It was stated that a consistent solution would require that the dipole-dipole interactions between the atoms be treated exactly.

In this paper, we provide such an exact solution. In other words, we do not make the RE approximation as in our previous paper. Moreover, we consider arrays of atoms at fixed positions, whereas the limit of a continuous atom density was taken in our previous work. We calculate the time-integrated, joint probability distribution for radiation to be emitted in a given direction and polarization on each transition and use this joint probability distribution to calculate the time-integrated intensity emitted on each transition. As in our previous calculation, we consider a cascade scheme in which the total angular momentum of the ground state is $J = 0$, that of the intermediate state is $J = 1$, and that of the upper state is $J = 0$ (see Fig. 1). The qualitative nature of the results will be the same for other values of the angular momenta. To introduce the concepts that are involved and the notation, we first analyze the radiation pattern for two atoms, for which analytic solutions can be obtained. We find that the radiation emitted on the upper transition is unpolarized and isotropic, as could have been predicted based on

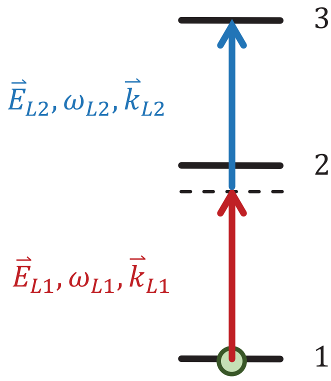

FIG. 1. Atomic energy level diagram of each atom in the ensemble. Levels 1 and 3 have total angular momentum $J = 0$, while level 2 has total angular momentum $J = 1$. Pulsed fields create a coherence between levels 1 and 3. The fields can be co- or counterpropagating. In the case of counterpropagating fields, it is assumed that $k_{L1} \approx k_{L2} \approx \omega_{32}/c \approx \omega_{21}/c$.

simple physical arguments. One of our principle goals is to show that, somewhat surprisingly, the radiation on the lower transition can also be isotropic and unpolarized, provided that the excitation fields are counterpropagating and that the ground-to-intermediate and intermediate-to-upper-level transition frequencies are nearly equal. The calculation is then extended formally to an ensemble of N fixed atoms at arbitrary positions. We determine conditions for which there can be a phase-matched enhancement of the joint probability density for specific directions of emission on the upper and lower transitions.

The N-atom formalism is used to obtain the emission pattern for an array of 20 atoms. It is shown that the RE approximation leads to very good agreement with the exact results for the joint probability density. Moreover, we show that the fraction of radiation emitted in the phase-matched directions by the array is similar to that of a medium characterized by a uniform atomic density, but there is an important difference. With copropagating excitation fields, the superradiant emission from a uniform density medium is confined to the forward direction (i.e., the same direction as the excitation fields), but the emission from an array can also occur for angles corresponding to Bragg resonances. We should note that the role of magnetic degeneracy on phase-matched cascade emission from a three-dimensional atomic array was considered by Miroshnychenko *et al.* [13], but in their case the upper transition was driven by a classical laser field. They showed that directional superradiant emission could be emitted by the sample on the lower transition.

II. TWO ATOMS

In an interaction representation, the Hamiltonian for the atom-vacuum field interaction for our system of two $J = 0 - 1 - 0$ three-level atoms is

$$H(t) = -i\left(\frac{\hbar\omega_{32}}{2\epsilon_0\mathcal{V}}\right)^{1/2}\sum_{\mathbf{k},\lambda}\sum_{j=1}^{2}\sum_{m=-1}^{1}\boldsymbol{\mu}_{3m}\cdot\boldsymbol{\epsilon}_{\mathbf{k}}^{(\lambda)}\sigma_{3m}^{(j)}a_{\mathbf{k}_\lambda}e^{i\mathbf{k}\cdot\mathbf{R}_j}e^{-i(\omega_k-\omega_{32})t}$$
$$-i\left(\frac{\hbar\omega_{21}}{2\epsilon_0\mathcal{V}}\right)^{1/2}\sum_{\mathbf{k},\lambda}\sum_{j=1}^{2}\sum_{m=-1}^{1}\boldsymbol{\mu}_{m1}\cdot\boldsymbol{\epsilon}_{\mathbf{k}}^{(\lambda)}\sigma_{m1}^{(j)}a_{\mathbf{k}_\lambda}e^{i\mathbf{k}\cdot\mathbf{R}_j}e^{-i(\omega_k-\omega_{21})t} + \text{adjoint}, \quad (1)$$

where $\boldsymbol{\mu}_{3m}$ is a dipole moment matrix element between states $|3\rangle$ and $|2m\rangle$, $\boldsymbol{\mu}_{m1}$ is a dipole moment matrix element between states $|2m\rangle$ and $|1\rangle$, $\sigma_{3m}^{(j)}$ and $\sigma_{m1}^{(j)}$ are atomic raising operators, $a_{\mathbf{k}_\lambda}$ is a field annihilation operator for a photon having propagation vector $\mathbf{k}$ and polarization $\lambda = (\hat{\boldsymbol{\theta}}, \hat{\boldsymbol{\phi}})$, $\mathbf{R}_j$ is the position of atom j, $\omega_k = kc$, ω_{32} and ω_{21} are the upper and lower transition frequencies, respectively,

$$\hat{\boldsymbol{\theta}} = \epsilon_{\mathbf{k}}^{(\theta)} = \cos\theta_k\cos\phi_k\hat{\mathbf{x}} + \cos\theta_k\sin\phi_k\hat{\mathbf{y}} - \sin\theta_k\hat{\mathbf{z}}, \quad (2)$$

$$\hat{\boldsymbol{\phi}} = \epsilon_{\mathbf{k}}^{(\phi)} = -\sin\phi_k\hat{\mathbf{x}} + \cos\phi_k\hat{\mathbf{y}}, \quad (3)$$

$$\hat{\mathbf{k}} = \sin\theta_k\cos\phi_k\hat{\mathbf{x}} + \sin\theta_k\sin\phi_k\hat{\mathbf{y}} + \cos\theta_k\hat{\mathbf{z}}, \quad (4)$$

θ_k and ϕ_k spherical coordinates, $\mathcal{V}$ is the quantization volume, and we have evaluated the radiated field frequencies at the atomic transition frequencies.

Each atom is assumed to have been prepared in a superposition of levels 1 and 3. We consider an initial state vector for which there is a phased, single excitation in the ensemble,

$$|\psi(0)\rangle = c_{31}(0)|31\rangle e^{i\boldsymbol{\kappa}\cdot\mathbf{R}_1} + c_{13}(0)|13\rangle e^{i\boldsymbol{\kappa}\cdot\mathbf{R}_2}, \quad (5)$$

where $\boldsymbol{\kappa} = \mathbf{k}_{L1} + \mathbf{k}_{L2}$; $\mathbf{k}_{L1}$ and $\mathbf{k}_{L2}$ are propagation vectors of the two laser fields used to generate the initial state; $|31\rangle$ is the state in which atom 1 is in state 3, atom 2 is in state 1, and the radiation field in its vacuum state; $|13\rangle$ is the state in which atom 1 is in state 1, atom 2 is in state 3, and the radiation field in its vacuum state; and $c_{31}(0)$ and $c_{13}(0)$ are the corresponding initial state amplitudes satisfying

$$|c_{31}(0)|^2 + |c_{13}(0)|^2 = 1. \quad (6)$$

For a symmetric phased state,

$$c_{31}^{\text{sym}}(0) = c_{13}^{\text{sym}}(0) = 1/\sqrt{2}. \quad (7)$$

To further simplify matters, we shall assume that the excitation fields are either co- or counterpropagating along the z axis,

$$\boldsymbol{\kappa} = \mathbf{k}_{L1} + \mathbf{k}_{L2} = (k_{L1} \pm k_{L2})\hat{\mathbf{z}}; \quad (8)$$

that the fields are in two-photon resonance with the $1 - 3$ transition,

$$\omega_{L1} + \omega_{L2} = \omega_{32} + \omega_{21} = \omega_{31}; \quad (9)$$

and that both $c_{31}(0)$ and $c_{13}(0)$ are real. We set $\mathbf{R}_1 = 0\hat{\mathbf{z}}$ and $\mathbf{R}_2 = Z_0\hat{\mathbf{z}}$, with $Z_0 > 0$.

For the initial state vector given in Eq. (5), we can write the state vector at any time as

$$\begin{aligned}|\psi(t)\rangle &= c_{31}(t)|31\rangle e^{-i\omega_{31}t} + c_{13}(t)|13\rangle e^{-i\omega_{31}t} \\ &\quad + \sum_{\mathbf{k}_A^\lambda} c_{m1;\mathbf{k}_A^\lambda}(t)\big|m1;\mathbf{k}_A^\lambda\big\rangle e^{-i(\omega_{21}+\omega_{k_A})t} \\ &\quad + \sum_{\mathbf{k}_A^\lambda} c_{1m;\mathbf{k}_A^\lambda}(t)\big|1m;\mathbf{k}_A^\lambda\big\rangle e^{-i(\omega_{21}+\omega_{k_A})t} \\ &\quad + \sum_{\mathbf{k}_A^\lambda,\mathbf{k}_B^{\lambda'}} c_{\mathbf{k}_A^\lambda,\mathbf{k}_B^{\lambda'}}(t)\big|\mathbf{k}_A^\lambda,\mathbf{k}_B^{\lambda'}\big\rangle e^{-i(\omega_{k_B}+\omega_{k_A})t}, \end{aligned} \tag{10}$$

where $|1m;\mathbf{k}_A^\lambda\rangle$ is the ket corresponding to atom 1 in state 1, atom 2 in sublevel m of level 2, and a photon $\mathbf{k}_A^\lambda$ in the radiation field; $|m1;\mathbf{k}_A^\lambda\rangle$ is the ket corresponding to atom 1 in sublevel m of level 2, atom 2 in state 1, and a photon $\mathbf{k}_A^\lambda$ in the radiation field; $|\mathbf{k}_A^\lambda,\mathbf{k}_B^{\lambda'}\rangle$ is the ket corresponding to both atoms in state 1 and photons $\mathbf{k}_A^\lambda$ and $\mathbf{k}_B^{\lambda'}$ in the radiation field; and $k_A = \omega_{k_A}/c \approx \omega_{32}/c = k_{32}$, $k_B = \omega_{k_B}/c \approx \omega_{21}/c = k_{21}$. The superscript λ refers to the polarization of the field. Using the Hamiltonian given in Eq. (1), we can obtain evolution equations for the state amplitudes. Following the standard approach used in theories of spontaneous emission involving two atoms [14], it is then possible to write the evolution equations for the state amplitudes as

$$\dot{c}_{31} = -\frac{\gamma_3}{2}c_{31}; \quad \dot{c}_{13} = -\frac{\gamma_3}{2}c_{13}, \tag{11a}$$

$$\begin{aligned}\dot{c}_{m1;\mathbf{k}_A^\lambda} &= -\left(\frac{\gamma_2}{2}\right)c_{m1;\mathbf{k}_A^\lambda} - \frac{\gamma_2(p_m+iq_m)}{2}c_{1m;\mathbf{k}_A^\lambda} \\ &\quad + \left(\frac{1}{i\hbar}\right)H^{(1)}_{m\mathbf{k}_A^\lambda,3}e^{-i(\omega_{32}-\omega_{k_A})t}c_{31},\end{aligned} \tag{11b}$$

$$\begin{aligned}\dot{c}_{1m;\mathbf{k}_A^\lambda} &= -\left(\frac{\gamma_2}{2}\right)c_{1m;\mathbf{k}_A^\lambda} - \frac{\gamma_2(p_m+iq_m)}{2}c_{m1;\mathbf{k}_A^\lambda} \\ &\quad + \left(\frac{1}{i\hbar}\right)H^{(2)}_{m\mathbf{k}_A^\lambda,3}e^{-i(\omega_{32}-\omega_{k_A})t}c_{13},\end{aligned} \tag{11c}$$

$$\dot{c}_{\mathbf{k}_A^\lambda,\mathbf{k}_B^{\lambda'}} = \frac{1}{i\hbar}\big[H^{(1)}_{1\mathbf{k}_B^{\lambda'},m}c_{m1;\mathbf{k}_A^\lambda} + H^{(2)}_{1\mathbf{k}_B^{\lambda'},m}c_{1m;\mathbf{k}_A^\lambda}\big]e^{-i(\omega_{21}-\omega_{k_B})t}, \tag{11d}$$

where

$$p_{\pm1}(\xi) = \frac{3}{2}\left\{\frac{\sin\xi}{\xi} + \left(\frac{\cos\xi}{\xi^2} - \frac{\sin\xi}{\xi^3}\right)\right\}, \tag{12a}$$

$$q_{\pm1}(\xi) = \frac{3}{2}\left\{-\frac{\cos\xi}{\xi} + \left(\frac{\sin\xi}{\xi^2} + \frac{\cos\xi}{\xi^3}\right)\right\}, \tag{12b}$$

$$p_0(\xi) = -3\left(\frac{\cos\xi}{\xi^2} - \frac{\sin\xi}{\xi^3}\right), \tag{13a}$$

$$q_0(\xi) = -3\left(\frac{\sin\xi}{\xi^2} + \frac{\cos\xi}{\xi^3}\right), \tag{13b}$$

the free space decay rates are

$$\gamma_3 = \frac{\omega_{32}^3|\langle 2\|\mu\|3\rangle|^2}{3\pi\epsilon_0\hbar c^3}, \tag{14}$$

$$\gamma_2 = \frac{\omega_{21}^3|\langle 1\|\mu\|2\rangle|^2}{9\pi\epsilon_0\hbar c^3}, \tag{15}$$

$\langle 2\|\mu\|3\rangle$ and $\langle 1\|\mu\|2\rangle$ are reduced matrix elements of the dipole moment operator, and

$$\xi = k_{21}Z_0.$$

We assume that $\hat{\mathbf{k}}_A$ is characterized by spherical coordinates $\Omega_A = (\theta_A,\phi_A)$ and $\hat{\mathbf{k}}_B$ by spherical coordinates $\Omega_B = (\theta_B,\phi_B)$. In that case, the matrix elements appearing in Eqs. (11) are

$$H^{(j)}_{m\mathbf{k}_A^\lambda,3} = i\left(\frac{\hbar\omega_{32}}{2\epsilon_0\mathcal{V}}\right)^{1/2}\langle 2\|\mu\|3\rangle H^\lambda_{Am}(\Omega_A)e^{-i\mathbf{k}_A\cdot\mathbf{R}_j}, \tag{16a}$$

$$H^{(j)}_{1\mathbf{k}_B^\lambda,m} = i\left(\frac{\hbar\omega_{21}}{2\epsilon_0\mathcal{V}}\right)^{1/2}\langle 1\|\mu\|2\rangle H^\lambda_{Bm}(\Omega_B)e^{-i\mathbf{k}_B\cdot\mathbf{R}_j}, \tag{16b}$$

where values for $H^\lambda_{Am}(\Omega_A)$ and $H^\lambda_{Bm}(\Omega_B)$ are listed in Appendix A.

The solution of Eq. (11a) is

$$c_{31}(t) = c_{31}(0)e^{-\gamma_3 t/2}, \qquad c_{13}(t) = c_{13}(0)e^{-\gamma_3 t/2}e^{i\kappa Z_0}, \tag{17}$$

which, when substituted into Eqs. (11), allows us to calculate

$$\begin{aligned}c_{1m;\mathbf{k}_A^\lambda}(t) &= \left(\frac{1}{2i\hbar}\right)\big[H^{(1)}_{m\mathbf{k}_A^\lambda,3}A_m(t)c_{31}(0) \\ &\quad + H^{(2)}_{m\mathbf{k}_A^\lambda,3}B_m(t)e^{i\kappa Z_0}c_{13}(0)\big],\end{aligned} \tag{18a}$$

$$\begin{aligned}c_{m1;\mathbf{k}_A^\lambda}(t) &= \left(\frac{1}{2i\hbar}\right)\big[H^{(2)}_{m\mathbf{k}_A^\lambda,3}A_m(t)e^{i\kappa Z_0}c_{13}(0) \\ &\quad + H^{(1)}_{m\mathbf{k}_A^\lambda,3}B_m(t)c_{31}(0)\big],\end{aligned} \tag{18b}$$

$$\begin{aligned}c_{\mathbf{k}_A^\lambda,\mathbf{k}_B^{\lambda'}}(\infty) &= \frac{1}{i\hbar}\int_0^\infty dt\big[H^{(1)}_{1\mathbf{k}_B^{\lambda'},m}c_{m1;\mathbf{k}_A^\lambda}(t) + H^{(2)}_{1\mathbf{k}_B^{\lambda'},m}c_{1m;\mathbf{k}_A^\lambda}(t)\big] \\ &\quad \times e^{-i(\omega_{21}-\omega_{k_B})t},\end{aligned} \tag{18c}$$

where

$$\begin{aligned}A_m(t) &= \int_0^t dt' e^{-i(\omega_{32}-\omega_{k_A})t'}e^{-\gamma_3 t'/2} \\ &\quad \times \big[e^{-(\gamma_2+\gamma_m)(t-t')/2} + e^{-(\gamma_2-\gamma_m)(t-t')/2}\big],\end{aligned} \tag{19a}$$

$$\begin{aligned}B_m(t) &= \int_0^t dt' e^{-i(\omega_{32}-\omega_{k_A})t'}e^{-\gamma_3 t'/2} \\ &\quad \times \big[e^{-(\gamma_2+\gamma_m)(t-t')/2} - e^{-(\gamma_2-\gamma_m)(t-t')/2}\big].\end{aligned} \tag{19b}$$

The joint probability per unit solid angle squared, $P(\boldsymbol{\alpha}_A,\boldsymbol{\alpha}_B;\Omega_A,\Omega_B)$, to emit [a photon on the upper transition having polar coordinates $\Omega_A = (\theta_A,\phi_A)$ and polarization $\boldsymbol{\alpha}_A = \hat{\boldsymbol{\theta}}_A,\hat{\boldsymbol{\phi}}_A$] + [a photon on the lower transition having polar coordinates $\Omega_B = (\theta_B,\phi_B)$ and polarization $\boldsymbol{\alpha}_B = \hat{\boldsymbol{\theta}}_B,\hat{\boldsymbol{\phi}}_B$] is given by

$$\begin{aligned}P(\boldsymbol{\alpha}_A,\boldsymbol{\alpha}_B;\Omega_A,\Omega_B) &\approx \frac{\mathcal{V}\omega_{21}^2\omega_{32}^2}{\hbar^4(2\pi c)^6} \\ &\quad \times \int_0^\infty d\omega_{k_B}\int_0^\infty d\omega_{k_A}\big|c_{\mathbf{k}_A^{\alpha_A},\mathbf{k}_B^{\alpha_B}}(\infty)\big|^2,\end{aligned} \tag{20}$$

where

$$\hat{\boldsymbol{\theta}}_\alpha = \cos\theta_\alpha \cos\phi_\alpha \hat{\mathbf{x}} + \cos\theta_\alpha \sin\phi_\alpha \hat{\mathbf{y}} - \sin\theta_\alpha \hat{\mathbf{z}}, \tag{21}$$

$$\hat{\boldsymbol{\phi}}_\alpha = -\sin\phi_\alpha \hat{\mathbf{x}} + \cos\phi_\alpha \hat{\mathbf{y}}, \tag{22}$$

for $\alpha = A, B$. There is now a lot of algebra involved to obtain the final expressions for $c_{\mathbf{k}_A^\lambda,\mathbf{k}_B^{\lambda'}}(\infty)$ and $P(\boldsymbol{\alpha}_A, \boldsymbol{\alpha}_B; \Omega_A, \Omega_B)$. Within the Weisskopf-Wigner approximation (evaluating frequencies appearing as factors in Eq. (20) at the atomic transition frequencies, and extending the integrals over ω_{k_B} and ω_{k_A} to $-\infty$), we find

$$P(\boldsymbol{\alpha}_A, \boldsymbol{\alpha}_B; \Omega_A, \Omega_B) = \frac{3}{64\pi^2}\big[F_1 J_{\boldsymbol{\alpha}_A,\boldsymbol{\alpha}_B} + F_2 K_{\boldsymbol{\alpha}_A,\boldsymbol{\alpha}_B} + F_3 L_{\boldsymbol{\alpha}_A,\boldsymbol{\alpha}_B} + F_4 M_{\boldsymbol{\alpha}_A,\alpha_\alpha}\big], \tag{23}$$

where expressions for F, J, K, L, and M are given in Appendix A.

With the equations given in Appendix A, it can be shown explicitly that probability is conserved,

$$\sum_{\boldsymbol{\alpha}_A,\boldsymbol{\alpha}_B} \int d\Omega_A \int d\Omega_B P(\boldsymbol{\alpha}_A, \boldsymbol{\alpha}_B; \Omega_A, \Omega_B) = 1, \tag{24}$$

and that the probability distribution $P_A(\boldsymbol{\alpha}_A, \Omega_A)$ for emission having polarization $\boldsymbol{\alpha}_A$ on the upper transition is isotropic and unpolarized,

$$P_A(\boldsymbol{\alpha}_A, \Omega_A) = \sum_{\boldsymbol{\alpha}_B} \int d\Omega_B P(\boldsymbol{\alpha}_A, \boldsymbol{\alpha}_B; \Omega_A, \Omega_B) = \frac{1}{8\pi}. \tag{25}$$

The fact that the radiation emitted on the upper transition is unpolarized and isotropic can be given a simple physical interpretation. Suppose atom 1 was in level 3 and atom 2 in level 2. As a result of the dipole-dipole interaction between the atoms induced by the vacuum field, the atoms could exchange their excitation, with atom 1 ending up in level 2 and atom 2 in level 3. However, with a *single* excitation in the system it is *impossible* to have one atom in level 2 and one in level 3. As a consequence, dipole-dipole interactions play no role in the emission process on the upper transition, and the radiation pattern on the upper transition is totally independent of any excitation exchange between the atoms that occurs on the lower transition. The radiation pattern on the upper transition is identical to that for a single atom, which is isotropic and unpolarized since level 3 has $J = 0$.

The probability distribution $P_B(\boldsymbol{\alpha}_B, \Omega_B)$ for emission on the lower transition is given by

$$P_B(\boldsymbol{\alpha}_B, \Omega_B) = \sum_{\boldsymbol{\alpha}_A} \int d\Omega_A P(\boldsymbol{\alpha}_A, \boldsymbol{\alpha}_B; \Omega_A, \Omega_B) = P_B(\boldsymbol{\alpha}_B, \theta_B); \tag{26}$$

that is, $P_B(\boldsymbol{\alpha}_B, \Omega_B)$ is a function of θ_B only, owing to the overall cylindrical symmetry of the excitation fields and atom geometry. In general, the radiation on the lower transition is polarized and anisotropic. There *is* one limit, however, in which the radiation emitted on the lower transition is unpolarized and isotropic. For $k_{21} = k_{32}$, $\kappa = 0$, $c_{31}(0) = c_{13}(0) = 1/\sqrt{2}$, we shall see that it is possible to prove that the radiation patterns on the upper and lower transitions are *identical*. Since the radiation pattern on the upper transition is isotropic and unpolarized, it follows that the radiation pattern on the lower transition is also isotropic and unpolarized .

A. Examples

To reduce the number of free parameters in the following examples, we shall take $k_{21}Z_0 = k_{32}Z_0 = \xi = 8$, and $\kappa Z_0 = 2\xi$ (copropagating excitation fields), or $\kappa Z_0 = 0$ (counterpropagating excitation fields). In general, for this value of ξ, there will be a number of Bragg-like resonances for various values of Ω_A and Ω_B. For comparison's sake, it will be helpful to recall that, for a single atom,

$$P^{(s)}(\boldsymbol{\alpha}_A, \boldsymbol{\alpha}_B; \Omega_A, \Omega_B) = \frac{3}{64\pi^2}\Pi_{\boldsymbol{\alpha}_A,\boldsymbol{\alpha}_B}(\Omega_A, \Omega_B), \tag{27}$$

where

$$\Pi_{\hat{\boldsymbol{\theta}}_A,\hat{\boldsymbol{\theta}}_B}(\Omega_A, \Omega_B) = [\cos\theta_A \cos\theta_B \cos(\phi_A - \phi_B) + \sin\theta_A \sin\theta_B]^2, \tag{28a}$$

$$\Pi_{\hat{\boldsymbol{\theta}}_A,\hat{\boldsymbol{\phi}}_B}(\Omega_A, \Omega_B) = \cos^2\theta_A \sin^2(\phi_A - \phi_B), \tag{28b}$$

$$\Pi_{\hat{\boldsymbol{\phi}}_A,\hat{\boldsymbol{\theta}}_B}(\Omega_A, \Omega_B) = \cos^2\theta_B \sin^2(\phi_A - \phi_B), \tag{28c}$$

$$\Pi_{\hat{\boldsymbol{\phi}}_A,\hat{\boldsymbol{\phi}}_B}(\Omega_A, \Omega_B) = \cos^2(\phi_A - \phi_B). \tag{28d}$$

1. Copropagating excitation fields

For copropagating fields, we expect that $P(\boldsymbol{\alpha}_A, \boldsymbol{\alpha}_B; \Omega_A, \Omega_B)$ has a constructive interference maximum when $\theta_A = \theta_B = 0$. For a single excitation in an ensemble of N atoms and $\xi \gg 1$, constructive interference can result in an N-fold increase in the probabilities over the single-atom result (it is not an N^2 increase, since the probability is multiplied by the initial state probabilities, which vary as $1/N$). This feature is seen in Figs. 2(a) and 2(b), where $P(\hat{\boldsymbol{\theta}}_A, \hat{\boldsymbol{\theta}}_B; \Omega_A, \Omega_B)$ and $P(\hat{\boldsymbol{\phi}}_A, \hat{\boldsymbol{\phi}}_B; \Omega_A, \Omega_B)$ are plotted as a function of θ_B for $\Omega_A = (0, 0)$, $\Omega_B = (\theta_B, 0)$, and $c_{31}(0) = c_{13}(0) = 1/\sqrt{2}$. The dashed curves in these figures are the corresponding single-atom results. Note the ratio of the two probabilities at $\Omega_A = \Omega_B = (0, 0)$ is approximately equal to 2.

In Figs. 2(c) and 2(d), we plot $P(\hat{\boldsymbol{\theta}}_A, \hat{\boldsymbol{\theta}}_B; \Omega_A, \Omega_B)$ and $P(\hat{\boldsymbol{\phi}}_A, \hat{\boldsymbol{\phi}}_B; \Omega_A, \Omega_B)$ as a function of θ_B for $\Omega_A = (\pi/2, 0)$, $\Omega_B = (\theta_B, 0)$, and $c_{31}(0) = c_{13}(0) = 1/\sqrt{2}$. There is no longer correlated phase-matched emission in the forward direction, but it is possible to get constructive interference for those values of θ_B corresponding to Bragg resonances.

In Fig. 3 we plot the probability densities $P_B(\hat{\boldsymbol{\theta}}_B; \theta_B)$ and $P_B(\hat{\boldsymbol{\phi}}_B; \theta_B)$ for the radiation pattern on the lower transition. As can be seen, the emission is both polarized and anisotropic.

2. Counterpropagating excitation fields

For counterpropagating fields with $k_B \approx k_A$ and $\kappa = 0$, $P(\hat{\boldsymbol{\theta}}_A, \hat{\boldsymbol{\theta}}_B; \Omega_A, \Omega_B)$ has a constructive interference maximum when $\theta_B = \pi - \theta_A$. That is, in contrast to the copropagating case, the constructive interference maximum occurs for any value Ω_A. This feature is seen in Figs. 4(a) and 4(b), where $P(\hat{\boldsymbol{\theta}}_A, \hat{\boldsymbol{\theta}}_B; \Omega_A, \Omega_B)$ and $P(\hat{\boldsymbol{\phi}}_A, \hat{\boldsymbol{\phi}}_B; \Omega_A, \Omega_B)$ are plotted as a function of θ_B for $\Omega_A = (0, 0)$, $\Omega_B = (\theta_B, 0)$, and $c_{31}(0) = c_{13}(0) = 1/\sqrt{2}$. The dashed curves in these figures are the

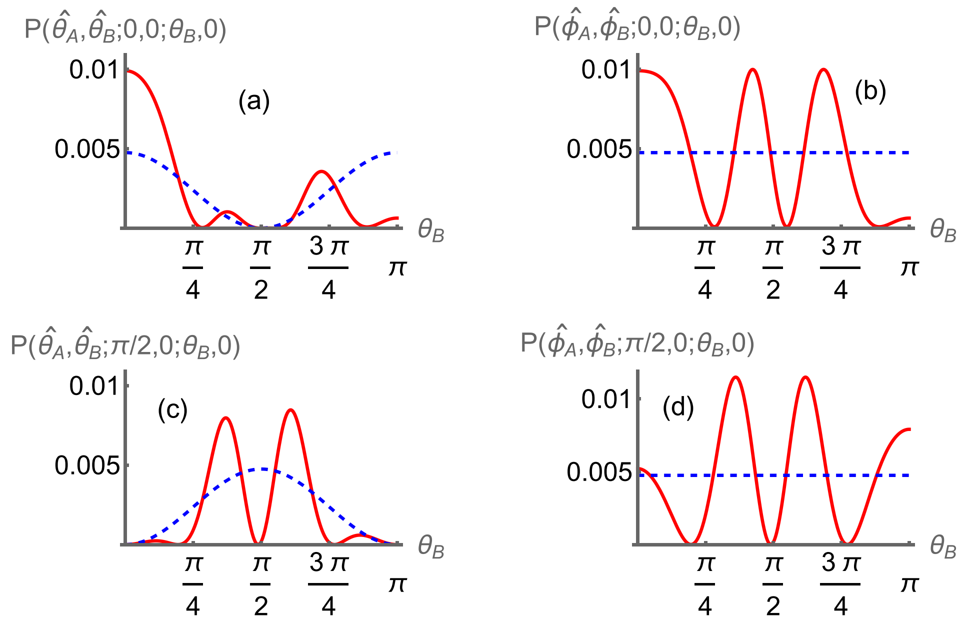

FIG. 2. Joint probability density $P(\hat{\boldsymbol{\theta}}_A, \hat{\boldsymbol{\theta}}_B; \Omega_A, \Omega_B)$ for copropagating excitation fields as a function of θ_B for $\xi = 8$, $\Omega_B = (\theta_B, 0)$, and $c_{31}(0) = c_{13}(0) = 1/\sqrt{2}$. (a) $\boldsymbol{\alpha}_A = \hat{\boldsymbol{\theta}}_A$, $\boldsymbol{\alpha}_B = \hat{\boldsymbol{\theta}}_B$, $\Omega_A = (0, 0)$; (b) $\boldsymbol{\alpha}_A = \hat{\boldsymbol{\phi}}_A$, $\boldsymbol{\alpha}_B = \hat{\boldsymbol{\phi}}_B$, $\Omega_A = (0, 0)$; (c) $\boldsymbol{\alpha}_A = \hat{\boldsymbol{\theta}}_A$, $\boldsymbol{\alpha}_B = \hat{\boldsymbol{\theta}}_B$, $\Omega_A = (\pi/2, 0)$; (d) $\boldsymbol{\alpha}_A = \hat{\boldsymbol{\phi}}_A$, $\boldsymbol{\alpha}_B = \hat{\boldsymbol{\phi}}_B$, $\Omega_A = (\pi/2, 0)$. The dashed curves are the single-atom result.

corresponding single-atom results. Note that the ratio of the two probabilities at $\Omega_B = (\pi, 0)$ is approximately equal to 2 and that there are additional Bragg resonances that also occur.

In Figs. 4(c) and 4(d) we plot $P(\hat{\boldsymbol{\theta}}_A, \hat{\boldsymbol{\theta}}_B; \Omega_A, \Omega_B)$ and $P(\hat{\boldsymbol{\phi}}_A, \hat{\boldsymbol{\phi}}_B; \Omega_A, \Omega_B)$ as a function of θ_B for $\Omega_A = (\pi/2, 0)$, $\Omega_B = (\theta_B, 0)$, and $c_{31}(0) = c_{13}(0) = 1/\sqrt{2}$. Now, the major constructive interference occurs for $\theta_B = \pi - \theta_A = \pi/2$, in addition to other Bragg resonances.

The probability densities $P_B(\hat{\boldsymbol{\theta}}_B; \theta_B)$ and $P_B(\hat{\boldsymbol{\phi}}_B; \theta_B)$ for the radiation pattern on the lower transition are both equal to $1/8\pi$ if $c_{31}(0) = c_{13}(0) = 1/\sqrt{2}$; that is, the emission is isotropic and unpolarized. In contrast, if we take as our initial condition $c_{31}(0) = 1$ and $c_{13}(0) = 0$, the symmetry is broken and the radiation pattern becomes polarized and anisotropic. This is seen in Fig. 5, where we plot $P_B(\hat{\boldsymbol{\theta}}_B; \theta_B)$ and $P_B(\hat{\boldsymbol{\phi}}_B; \theta_B)$ as a function of θ for $c_{31}(0) = 1$, $c_{13}(0) = 0$.

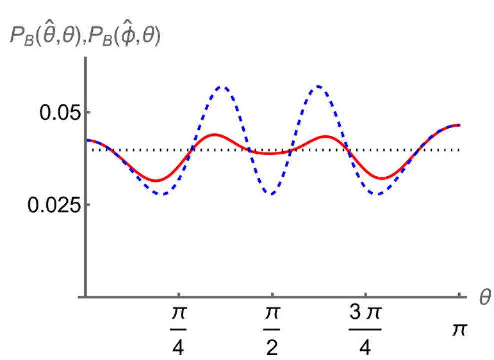

FIG. 3. Lower transition probability densities $P_B(\hat{\boldsymbol{\theta}}_B; \theta_B)$ and $P_B(\hat{\boldsymbol{\phi}}_B; \theta_B)$ for copropagating excitation fields as a function of θ_B for $\xi = 8$ and $c_{31}(0) = c_{13}(0) = 1/\sqrt{2}$. The dotted line is the single-atom result.

III. N ATOMS

The calculation can be extended, at least formally, to an ensemble of N fixed atoms. In an interaction representation, the Hamiltonian for N atoms is given by Eq. (1), with the sum over j extended from 2 to N. Each atom is assumed to have been prepared in a superposition of levels 1 and 3. We consider an initial state vector for which there is a phased, single excitation in the ensemble,

$$|\psi(0)\rangle = \sum_{j=-1}^{N} c_{j3}(0) e^{i\boldsymbol{\kappa}\cdot\mathbf{R}_j} |3_j\rangle, \tag{29}$$

where $|3_j\rangle$ is the state in which atom j is in state 3 and all the other atoms are in their ground state, $c_{j3}(0)$ is the initial state amplitude for atom j to be in level 3, and

$$\sum_{j=1}^{N} |c_{j3}(0)|^2 = 1. \tag{30}$$

For a symmetric phased state,

$$c_{j3}^{\text{sym}}(0) = 1/\sqrt{N}. \tag{31}$$

For this initial state vector, we can write the state vector at any time as

$$\begin{aligned} |\psi(t)\rangle = &\sum_{j=1}^{N} c_{j3}(t)|3_j\rangle e^{-i\omega_{31}t} \\ &+ \sum_{m=-1}^{1}\sum_{j=1}^{N}\sum_{\mathbf{k}_A^\lambda} c_{jm;\mathbf{k}_A^\lambda}(t)\big|m_j; \mathbf{k}_A^\lambda\big\rangle e^{-i(\omega_B+\omega_{k_A})t} \\ &+ \sum_{j=1}^{N}\sum_{\mathbf{k}_A^\lambda,\mathbf{k}_B^{\lambda'}} c_{\mathbf{k}_A^\lambda,\mathbf{k}_B^{\lambda'}}(t)\big|\mathbf{k}_A^\lambda, \mathbf{k}_B^{\lambda'}\big\rangle e^{-i(\omega_{k_B}+\omega_{k_A})t}, \end{aligned} \tag{32}$$

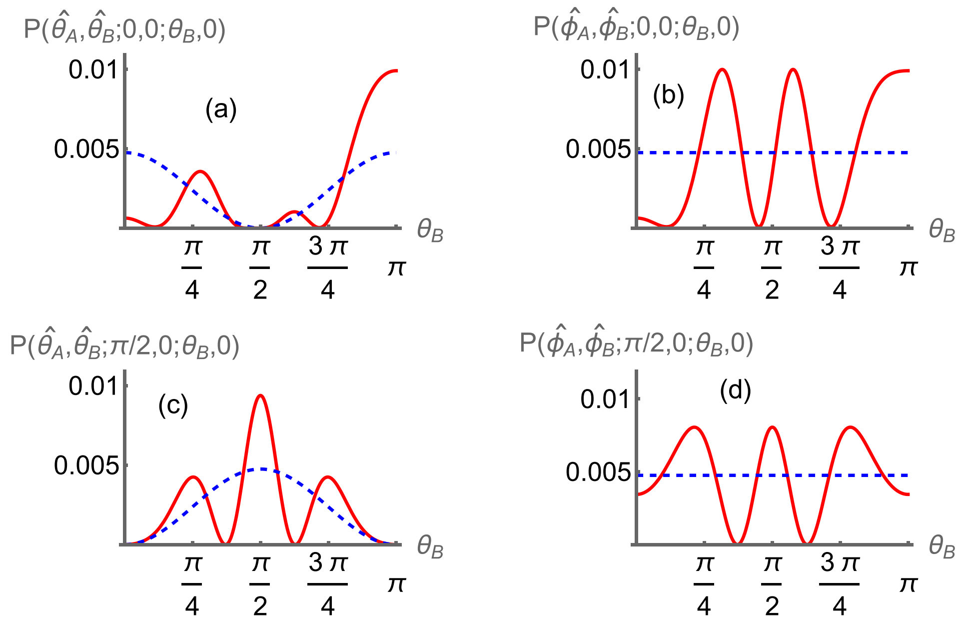

FIG. 4. Joint probability density $P(\hat{\boldsymbol{\theta}}_A, \hat{\boldsymbol{\theta}}_B; \Omega_A, \Omega_B)$ for counterpropagating excitation fields as a function of θ_B for $\xi = 8$, $\Omega_B = (\theta_B, 0)$, and $c_{31}(0) = c_{13}(0) = 1/\sqrt{2}$. (a) $\boldsymbol{\alpha}_A = \hat{\boldsymbol{\theta}}_A$, $\boldsymbol{\alpha}_B = \hat{\boldsymbol{\theta}}_B$, $\Omega_A = (0, 0)$; (b) $\boldsymbol{\alpha}_A = \hat{\boldsymbol{\phi}}_A$, $\boldsymbol{\alpha}_B = \hat{\boldsymbol{\phi}}_B$, $\Omega_A = (0, 0)$; (c) $\boldsymbol{\alpha}_A = \hat{\boldsymbol{\theta}}_A$, $\boldsymbol{\alpha}_B = \hat{\boldsymbol{\theta}}_B$, $\Omega_A = (\pi/2, 0)$; (d) $\boldsymbol{\alpha}_A = \hat{\boldsymbol{\phi}}_A$, $\boldsymbol{\alpha}_B = \hat{\boldsymbol{\phi}}_B$, $\Omega_A = (\pi/2, 0)$. The dashed curves are the single-atom result.

where $|m_j; \mathbf{k}_A^\lambda\rangle$ is a ket for atom j to be in sublevel m of level 2 and to have a photon emitted having propagation vector $\mathbf{k}_A$ and polarization λ, and $|\mathbf{k}_A^\lambda, \mathbf{k}_B^{\lambda'}\rangle$ is the ket corresponding to all atoms in level 1 and photons $\mathbf{k}_A^\lambda$ and $\mathbf{k}_B^{\lambda'}$ in the radiation field. The state amplitudes evolve as [14]

$$\dot{c}_{j3} = -\frac{\gamma_3}{2} c_{j3}, \tag{33a}$$

$$\begin{aligned}\dot{c}_{jm;\mathbf{k}_A^\lambda} = &-\frac{\gamma_2}{2} c_{jm;\mathbf{k}_A^\lambda} - \frac{\gamma_2}{2} \sum_{m=-1}^{1} \sum_{j'=1}^{N} (1 - \delta_{j,j'}) \\ &\times G_{mm'}(\mathbf{R}_{jj'}) c_{j'm';\mathbf{k}_A^\lambda} \\ &+ \left(\frac{1}{i\hbar}\right) H^{(j)}_{m\mathbf{k}_A^\lambda,3} e^{-i(\omega_{32}-\omega_{k_A})t} c_{j3}\end{aligned} \tag{33b}$$

$$\dot{c}_{\mathbf{k}_A^\lambda,\mathbf{k}_B^{\lambda'}} = \frac{1}{i\hbar} \sum_{m=-1}^{1} \sum_{j=1}^{N} H^{(j)}_{1\mathbf{k}_B^{\lambda'},m} c_{jm;\mathbf{k}_A^\lambda} e^{-i(\omega_{21}-\omega_{k_B})t}, \tag{33c}$$

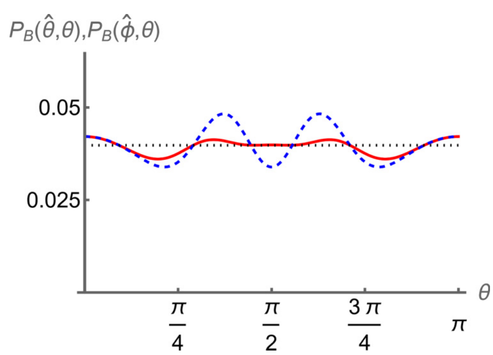

FIG. 5. Lower transition probability densities $P_B(\hat{\boldsymbol{\theta}}_B; \theta_B)$ and $P_B(\hat{\boldsymbol{\phi}}_B; \theta_B)$ for counterpropagating excitation fields as a function of θ_B for $\xi = 8$ and $c_{31}(0) = 1$; $c_{13}(0) = 0$. The dotted line is the single-atom result.

where the propagators

$$G_{mm'}(\mathbf{R}_{jj'}) = G_{mm'}(\mathbf{R}_{j'j}) \tag{34}$$

are listed in Appendix A and the H matrix elements are given by Eqs. (16).

We now define a $3N \times 3N$ *matrix* $\mathbf{G}$ having matrix elements

$$G_{jm;j'm'} = G_{mm'}(\mathbf{R}_{jj'})(1 - \delta_{j,j'}), \tag{35}$$

an intermediate state column vector $\mathbf{c}_2(t)$ having matrix elements $c_{jm;\mathbf{k}_A^\lambda}(t)$, and an initial state column vector $\mathbf{c}_0(t)$ having matrix elements $(\frac{1}{i\hbar}) H^{(j)}_{m\mathbf{k}_A^\lambda,3} e^{-i(\omega_A-\omega_{k_A})t} e^{i\boldsymbol{\kappa}\cdot\mathbf{R}_j} c_{j3}(0)$. The solution of Eq. (33b) is then

$$\mathbf{c}_2(t) = \int_0^t dt' \mathbf{V}(t - t') e^{-\gamma_3 t'/2} \mathbf{c}_0(t'), \tag{36}$$

where

$$\mathbf{V}(t) = e^{-\gamma_2 t/2} e^{-\gamma_2 \mathbf{G} t/2}, \tag{37}$$

having matrix elements $V_{jm,j'm'}$. The formal solution for $c_{\mathbf{k}_A^\lambda,\mathbf{k}_B^{\lambda'}}(\infty)$ is

$$\begin{aligned}c_{\mathbf{k}_A^\lambda,\mathbf{k}_B^{\lambda'}}(\infty) = &\frac{1}{i\hbar} \sum_{m=-1}^{1} \sum_{j=1}^{N} H^{(j)}_{1\mathbf{k}_B^{\lambda'},m} \\ &\times \int_0^\infty c_{jm;\mathbf{k}_A^\lambda}(t) e^{-i(\omega_{21}-\omega_{k_B})t} dt.\end{aligned} \tag{38}$$

In forming $\int_0^\infty d\omega_{k_B}\int_0^\infty d\omega_{k_A}|c_{\mathbf{k}_A^\lambda,\mathbf{k}_B^{\lambda'}}(\infty)|^2$, we encounter terms of the type

$$\int_0^\infty d\omega_{k_B}\int_0^\infty d\omega_{k_A}\int_0^\infty dt e^{-i(\omega_{21}-\omega_{k_B})t}\int_0^t dt' V_{im,jm'}(t-t')e^{-i(\omega_{32}-\omega_{k_A})t'}e^{-\gamma_3 t'/2}$$
$$\times\int_0^\infty dt'' e^{i(\omega_{21}-\omega_{k_B})t''}\int_0^{t''} dt'''[V_{i'\bar{m},j'\bar{m}'}(t''-t''')]^* e^{i(\omega_{32}-\omega_{k_A})t'''}e^{-\gamma_3 t'''/2}.$$

If the frequency integrals are extended to $-\infty$, this expression reduces to

$$4\pi^2\int_0^\infty dt\int_0^\infty dt''\int_0^t dt'\int_0^{t''} dt''' V_{im,jm'}(t-t')\big[V_{i'\bar{m},j'\bar{m}'}(t''-t''')\big]^*$$
$$\times\ e^{-\gamma_3 t'/2}e^{-\gamma_3 t'''/2}\delta(t-t'')\delta(t'-t''')=4\pi^2 V_{im,jm';i'\bar{m},j'\bar{m}'},\tag{39}$$

where

$$V(im,jm';i'\bar{m},j'\bar{m}')=\gamma_2\gamma_3\int_0^\infty dt\int_0^t dt' V_{im,jm'}(t-t')[V_{i'\bar{m},j'\bar{m}'}(t-t')]^* e^{-\gamma_3 t'}$$
$$=\int_0^\infty dx V_{im,jm'}\left(\frac{x}{\gamma_2}\right)\left[V_{i'\bar{m},j'\bar{m}'}\left(\frac{x}{\gamma_2}\right)\right]^*.\tag{40}$$

Combining Eqs. (36)–(40), we obtain

$$P(\boldsymbol{\alpha}_A,\boldsymbol{\alpha}_B;\Omega_A,\Omega_B)=\frac{27}{64\pi^2}H(\boldsymbol{\alpha}_A,\boldsymbol{\alpha}_B,\Omega_A,\Omega_B,m,m',\bar{m},\bar{m}')V(im,jm';i'\bar{m},j'\bar{m}')$$
$$\times F(k_{32},k_{21},\kappa,\Omega_A,\Omega_B,i,j,i',j')c_{j3}(0)[c_{j'3}(0)]^*,\tag{41}$$

where

$$H(\boldsymbol{\alpha}_A,\boldsymbol{\alpha}_B,\Omega_A,\Omega_B,m,m',\bar{m},\bar{m}')=H_{Bm}^{\boldsymbol{\alpha}_B}(\Omega_B)H_{Am'}^{\boldsymbol{\alpha}_A}(\Omega_A)\big[H_{B\bar{m}}^{\boldsymbol{\alpha}_B}(\Omega_B)H_{A\bar{m}'}^{\boldsymbol{\alpha}_A}(\Omega_A)\big]^*,\tag{42}$$

$$F(k_{32},k_{21},\kappa,\Omega_A,\Omega_B,i,j,i',j')=e^{i\kappa Z_{jj'}}e^{-ik_{21}\hat{\mathbf{k}}_B\cdot\mathbf{R}_{ii'}}e^{-ik_{32}\hat{\mathbf{k}}_A\cdot\mathbf{R}_{jj'}},\tag{43}$$

and

$$\mathbf{R}_{jj'}=\mathbf{R}_{j'}-\mathbf{R}_j.\tag{44}$$

A summation convention is used in Eq. (41), where all repeated indices are summed with the sums over $m,m',\bar{m},\bar{m}'$ going from -1 to 1 and the sums over i,j,i',j' going from 1 to N. It turns out that, for $kR_{jj'}\gg 1$, the major contributions to $P(\boldsymbol{\alpha}_A,\boldsymbol{\alpha}_B;\Omega_A,\Omega_B)$ originate from terms having $\{i=j,i'=j',m=m',\bar{m}=\bar{m}'\}$. In other words, the dominant contribution is from cascade emission in the same atom through the same magnetic sublevel (modified by dipole-dipole interactions).

The spatial phase factor defined in Eq. (43) is equal to unity when $i=j$ and $i'=j'$ for copropagating excitation fields if $\theta_A=\theta_B=0$ and for counterpropagating excitation fields if $(\theta_B=\pi-\theta_A,\phi_B=\phi_A+\pi)$. In summing over i,j,i',j' in Eq. (41), this can lead to an enhancement factor of N in the probability density over the single-atom result for a completely phased symmetric initial state, $c_{j3}(0)=1/\sqrt{N}$. In other words, the maximum constructive interference we can expect for $P(\boldsymbol{\alpha}_A,\boldsymbol{\alpha}_B;\Omega_A,\Omega_B)$ is N times the single-atom result.

Computationally, it becomes time consuming to evaluate Eq. (40) for even three atoms placed at arbitrary positions since it involves the diagonalization of a 9×9 matrix for each value of x. On the other hand, we might ask if there are any symmetry relations that can be used to determine whether or not the emission on the lower transition remains isotropic and unpolarized when $k_{21}=k_{32}=k$, $\kappa=0$, $c_{j3}(0)=1/\sqrt{N}$. For example, from symmetry considerations, it follows that

$$H(\boldsymbol{\alpha}_A,\boldsymbol{\alpha}_B,\Omega_A,\Omega_B,m,m',\bar{m},\bar{m}')=(-1)^{(m+m'+\bar{m}+\bar{m}')}H(\boldsymbol{\alpha}_A,\boldsymbol{\alpha}_B,\Omega_B,\Omega_A,-m',-m,-\bar{m}',-\bar{m}),\tag{45a}$$

$$F(k,k,0,\Omega_A,\Omega_B,i,j,i',j')=F(k,k,0,\Omega_B,\Omega_A,j,i,j',i'),\tag{45b}$$

$$G_{jm;j'm'}=(-1)^{(m+m')}G_{j,-m';j',-m}\tag{45c}$$

$$V(im,jm';i'\bar{m},j'\bar{m}')=(-1)^{(m+m'+\bar{m}+\bar{m}')}V(j,-m',i,-m;j',-\bar{m}',i',-\bar{m}).\tag{45d}$$

When these expressions are used in Eq. (41), we find that

$$P(\boldsymbol{\alpha}_A,\boldsymbol{\alpha}_B;\Omega_A,\Omega_B)=P(\boldsymbol{\alpha}_B,\boldsymbol{\alpha}_A;\Omega_B,\Omega_A),\tag{46}$$

which, in turn, implies that

$$P_A(\hat{\boldsymbol{\theta}}, \Omega) = \int d\Omega'[P(\hat{\boldsymbol{\theta}}, \hat{\boldsymbol{\theta}}'; \Omega, \Omega') + P(\hat{\boldsymbol{\theta}}, \hat{\boldsymbol{\phi}}'; \Omega, \Omega')]$$
$$= \int d\Omega'[P(\hat{\boldsymbol{\theta}}', \hat{\boldsymbol{\theta}}, ; \Omega', \Omega) + P(\hat{\boldsymbol{\phi}}', \hat{\boldsymbol{\theta}}; \Omega', \Omega)] = P_B(\hat{\boldsymbol{\theta}}, \Omega), \tag{47a}$$

$$P_A(\hat{\boldsymbol{\phi}}, \Omega) = \int d\Omega'[P(\hat{\boldsymbol{\phi}}, \hat{\boldsymbol{\theta}}'; \Omega, \Omega') + P(\hat{\boldsymbol{\phi}}, \hat{\boldsymbol{\phi}}'; \Omega, \Omega')]$$
$$= \int d\Omega'[P(\hat{\boldsymbol{\theta}}', \hat{\boldsymbol{\phi}}; \Omega', \Omega) + P(\hat{\boldsymbol{\phi}}', \hat{\boldsymbol{\phi}}; \Omega', \Omega)] = P_B(\hat{\boldsymbol{\phi}}, \Omega); \tag{47b}$$

that is, the polarizations and angular distributions on both transitions are *identical*. Since the upper state transition radiation is unpolarized and isotropic, it then follows that the lower transition radiation is also unpolarized and isotropic when $k_{21} = k_{32} = k$, $\kappa = 0$, $c_{j3}(0) = 1/\sqrt{N}$. In Appendix B, we present a direct calculation of $P_B(\hat{\boldsymbol{\phi}}, \Omega)$ for large interatomic separations in order to illustrate how the signal becomes unpolarized and isotropic in these limits.

A. Example

We can test to see if the superradiant directional emission found by Miroshnychenko *et al.* [13] also occurs for our level scheme. To do so, we consider an array of fixed atoms that are equally spaced in the x, y, and z directions. That is, atom j is specified by $\{n_x, n_y, n_z, d\}$ with

$$\mathbf{R}_j = d[(n_x - 1)\hat{\mathbf{x}} + (n_y - 1)\hat{\mathbf{y}} + (n_z - 1)\hat{\mathbf{z}}] \tag{48}$$

and $1 \leqslant n_q \leqslant N_q$ $(q = x, y, z)$. The total number of atoms in the array is given by $N = N_x N_y N_z$. To simplify matters, we restrict the discussion to $c_{j3}(0) = 1/\sqrt{N}$ and $k_{21} = k_{32} = k$.

Let us neglect interactions for the moment. In that case,

$$V(im, jm'; i'\bar{m}, j'\bar{m}') = \delta_{i,j}\delta_{m,m'}\delta_{i'j'}\delta_{\bar{m},\bar{m}'} \tag{49}$$

and Eq. (41) reduces to

$$P_0(\boldsymbol{\alpha}_A, \boldsymbol{\alpha}_B, ; \Omega_A, \Omega_B) = \frac{3}{64N\pi^2}\Pi_{\boldsymbol{\alpha}_A,\boldsymbol{\alpha}_B}(\Omega_A, \Omega_B)F(k, \kappa, \Omega_A, \Omega_B), \tag{50}$$

where

$$F(k, \kappa, \Omega_A, \Omega_B) = \frac{\sin^2\left[\frac{N_x kd}{2}(\sin\theta_A\cos\phi_A + \sin\theta_B\cos\phi_B)\right]}{\sin^2\left[\frac{kd}{2}(\sin\theta_A\cos\phi_A + \sin\theta_B\cos\phi_B)\right]} \times \frac{\sin^2\left[\frac{N_y kd}{2}(\sin\theta_A\sin\phi_A + \sin\theta_B\sin\phi_B)\right]}{\sin^2\left[\frac{kd}{2}(\sin\theta_A\sin\phi_A + \sin\theta_B\sin\phi_B)\right]} \times \frac{\sin^2\left[\frac{N_z kd}{2}(\cos\theta_A + \cos\theta_B - \kappa/k)\right]}{\sin^2\left[\frac{kd}{2}(\cos\theta_A + \cos\theta_B - \kappa/k)\right]} \tag{51}$$

and the $\Pi_{\boldsymbol{\alpha}_A,\boldsymbol{\alpha}_B}(\Omega_A, \Omega_B)$ are given in Eqs. (28). Most of the directional properties of the emission are determined by the factor $F(k, \kappa, \Omega_A, \Omega_B)$. We note immediately that, for counterpropagating fields ($\kappa = 0$), the principal resonance occurs only for $\theta_B = \pi - \theta_A$, $\phi_B = \phi_A + \pi$. That is, in contrast to the two-atom case (or for N atoms on a line) where constructive interference occurs for any value of ϕ provided that $\theta_B = \pi - \theta_A$, the principal resonance for a three-dimensional array with $k_{21} = k_{32}$ occurs only if the fields radiated on the upper and lower transitions propagate in opposite directions.

To illustrate the physics, we now consider only copropagating fields ($\kappa = 2k$) and calculate the joint probability density as a function of Ω_B when $\Omega_A = (0, 0)$. In that limit,

$$F(k, 2k, 0, \Omega_B) = \frac{\sin^2\left[\frac{N_x kd}{2}\sin\theta_B\cos\phi_B\right]}{\sin^2\left[\frac{kd}{2}\sin\theta_B\cos\phi_B\right]} \times \frac{\sin^2\left[\frac{N_y kd}{2}\sin\theta_B\sin\phi_B\right]}{\sin^2\left[\frac{kd}{2}\sin\theta_B\sin\phi_B\right]} \times \frac{\sin^2\left[\frac{N_z kd}{2}(1 - \cos\theta_B)\right]}{\sin^2\left[\frac{kd}{2}(1 - \cos\theta_B)\right]}. \tag{52}$$

We can understand the qualitative nature of the result if we set $\phi_B = 0$. The principle phase-matched emission occurs for $\theta_B = 0$, resulting in $F = N^2$. Secondary Bragg resonances can occur if either or both of $\frac{kd}{2}\sin\theta_B$ or $\frac{kd}{2}(1 - \cos\theta_B)$ is an integral multiple of π, but, in general, their amplitude is less than that of the principal resonance. If both are integral multiples of π, as could be the case if kd is an integral multiple of 2π and $\theta_B = \pi/2$ or π, then $F = N^2$, the same amplitude as that of the principle phase-matched signal.

The expression given in Eq. (50) is essentially the RE approximation, when divided by a normalization constant

$$W(\Omega_A) = \Gamma_2(\Omega_A)/\gamma_2 = 4\pi \sum_{\boldsymbol{\alpha}_A,\boldsymbol{\alpha}_B} \int d\Omega_B P_0(\boldsymbol{\alpha}_A, \boldsymbol{\alpha}_B; \Omega_A, \Omega_B), \tag{53}$$

where $\Gamma_2(\Omega_A)$ is some effective decay constant for the array that depends on the direction of observation of the first photon. For example, with $N_x = 2$, $N_y = 2$, $N_z = 5$ ($N = 20$), and $kd = 5$, $\Gamma_2[\Omega_A = (0, 0)]/\gamma_2 = 1.19$, a decay rate that is somewhat superradiant.

We now look at the corresponding exact result, including interactions, for the same parameters. If $kR_{jj'} \geqslant 5$, it becomes computationally efficient to replace the exponential in Eq. (37) with its series expansion. It is then possible to carry

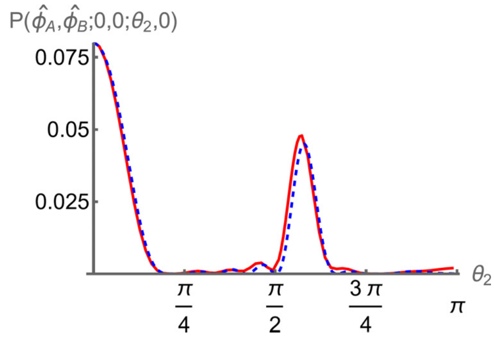

FIG. 6. Joint probability density $P(\hat{\boldsymbol{\phi}}_A, \hat{\boldsymbol{\phi}}_B; \Omega_A, \Omega_B)$ for an array of 20 atoms ($2 \times 2 \times 5$) for copropagating excitation fields as a function of θ_B for $kd = 5$, $\Omega_A = (0, 0)$, $\Omega_B = (\theta_B, 0)$, and $c_{j3}(0) = 1/\sqrt{20}$. The dashed line is the Rehler-Eberly approximation, given by Eq. (55).

out the integration over time in Eq. (40) to arrive at

$$\begin{aligned}
&V(im, jm'; i'\bar{m}, j'\bar{m}') \\
&= \gamma_2\gamma_3 \int_0^\infty dt \int_0^t dt' V_{im,jm'}(t-t')[V_{i'\bar{m},j'\bar{m}'}(t-t')]^* e^{-\gamma_3 t'} \\
&= \sum_{p=0}^{p_{\max}} \sum_{q=0}^{p} \binom{p}{q} \left(\frac{\gamma_2}{2}\right)^q (V^q)_{im,jm'} (V^{p-q})_{i'\bar{m},j'\bar{m}'}, \qquad (54)
\end{aligned}$$

where $\binom{p}{q}$ is a binomial coefficient and $p_{\max}$ is chosen to assure convergence. In Fig. 6, the solid red curve is a plot $P(\hat{\boldsymbol{\theta}}_A, \hat{\boldsymbol{\theta}}_B; \Omega_A, \Omega_B)$ as a function of θ_B for $N_x = 2$, $N_y = 2$, $N_z = 5$, $kd = 5$, and $c_{j3}(0) = 1/\sqrt{20}$ with $p_{\max} = 8$. The principle phase-matched resonance at $\theta_B = 0$ is seen, as is the Bragg resonance that occurs for

$$\frac{kd}{2}(1 - \cos\theta_B) = \frac{5}{2}(1 - \cos\theta_B) = \pi,$$

or $\theta_B \approx 1.83$. The fraction of correlated radiation emitted in the forward, phase-matched direction is 0.455 and the fraction of energy in the Bragg peak is 0.484. The fraction of energy in both peaks is about 0.94. That is, most of the signal originates from the phase-matched contributions, even if the emission is only slightly superradiant ($\Gamma_2[\Omega_A = (0, 0)]/\gamma_2 = 1.19$). In other words, we must distinguish between *spatial* superradiance and *temporal* superradiance. For example, in typical phase-matched coherent transients there is spatial superradiance since the signal is proportional to N^2 in the phase-matched direction, but there is essentially no temporal superradiance since the excitation decay rate is approximately that of a single atom.

In Fig. 6, the dashed curve is the normalized joint probability density,

$$\tilde{P}_0(\boldsymbol{\phi}_A, \boldsymbol{\phi}_B; 0, 0; \theta_B, 0) = P_0(\boldsymbol{\phi}_A, \boldsymbol{\phi}_B; 0, 0; \theta_B, 0)/1.19. \qquad (55)$$

As can be seen, the RE approximation provides a very good approximation to the exact result for the joint probability density. As such, one can get a good idea of the features of the joint probability distribution without carrying out extensive calculations. However, if we were to calculate the upper state probability density $P_A(\boldsymbol{\alpha}_A, \Omega)$ given by Eq. (25) using $\tilde{P}_0(\boldsymbol{\alpha}_A; \Omega_A)$, we would find that it incorrectly leads to a signal that is polarized and anisotropic, whereas the exact result $P_A(\boldsymbol{\alpha}_A; \Omega_A)$ leads to a signal that is isotropic and unpolarized. Moreover, if we were to calculate the radiation pattern for emission on the lower transition for counterpropagating excitation fields with $k_{21} = k_{32} = k$, $\kappa = 0$, and $c_{j3}(0) = 1/\sqrt{N}$, we would find that it is unpolarized, but anisotropic, whereas the exact radiation pattern is both unpolarized and isotropic.

The RE approximation can be used to get a good idea of the emission pattern when the number of atoms in each direction is much greater than unity. As an example, consider

$$\begin{aligned}
\tilde{P}_0(\boldsymbol{\phi}_A, \boldsymbol{\phi}_B; 0, 0; \theta_B, 0) &= \frac{3}{64 N_x N_z \pi^2} \frac{\sin^2\left[\frac{N_x kd}{2}\sin\theta_B\right]}{\sin^2\left[\frac{kd}{2}\sin\theta_B\right]} \\
&\quad \times \frac{\sin^2\left[\frac{N_z kd}{2}(1-\cos\theta_B)\right]}{\sin^2\left[\frac{kd}{2}(1-\cos\theta_B)\right]},
\end{aligned}$$

when both N_x and N_z are much greater than unity. In this limit, the value of $\tilde{P}_0(\boldsymbol{\phi}_A, \boldsymbol{\phi}_B; 0, 0; \theta_B, 0)$ is negligibly small, except at positions of the resonances. In other words, the correlated signal is confined to the phase-matched peaks. Moreover, if kd is not a multiple of 2π, the amplitude of the principal resonance at $\theta_B = 0$ is N_x or N_z times larger than that of the Bragg resonances. However, unless $N_z \gg N_x^2$, the principal resonance will contain only about 50% of the signal, since the width of the Bragg resonance is larger than that of the principal resonance. For example, when $N_x = 8$, $N_z = 20$, and $kd = 10$, the principal resonance contains about 47% of the signal. On the other hand, when $N_x = 8$, $N_z = 200$, and $kd = 10$, it contains about 90% of the signal and the emission is temporally superradiant ($\Gamma_2[\Omega_A = (0, 0)]/\gamma_2 = 6.65$)

B. *N* Atoms on a line

The problem simplifies considerably when all the atoms are located on the z axis. In that case, excitation exchange occurs only between magnetic sublevels of different atoms having the same magnetic quantum number. As a consequence, the $G_{jm,j'm'}$ are proportional to $\delta_{m,m'}$ and the $V(im, jm'; i'\bar{m}, j'\bar{m}')$ to $\delta_{m,m'}\delta_{\bar{m},\bar{m}'}$. As a consequence, Eq. (41) reduces to

$$\begin{aligned}
&P(\boldsymbol{\alpha}_A, \boldsymbol{\alpha}_B; \Omega_A, \Omega_B) \\
&\quad = \frac{27}{64\pi^2} H(\boldsymbol{\alpha}_A, \boldsymbol{\alpha}_B, \Omega_A, \Omega_B, m, m, m', m') \\
&\quad \times V(im, jm; i'm', j'm') \\
&\quad \times F(k_{32}, k_{21}, \kappa, \Omega_A, \Omega_B, i, j, i', j') c_{j3}(0)[c_{j'3}(0)]^*, \qquad (56)
\end{aligned}$$

with

$$\begin{aligned}
&F(k_{32}, k_{21}, \kappa, \Omega_A, \Omega_B, i, j, i', j') \\
&\quad = e^{i\kappa Z_{jj'}} e^{-ik_{21} Z_{ii'}\cos\theta_B} e^{-ik_{32} Z_{jj'}\cos\theta_A}. \qquad (57)
\end{aligned}$$

In the examples below, we set $k_{21} = k_{32} = k$, and $\kappa = 2k$ (copropagating excitation fields), or $\kappa = 0$ (counterpropagating excitation fields). We limit the calculation to an array of N atoms equally spaced along the z axis, with a separation d between adjacent atoms, and define $\xi = kd$. The initial state

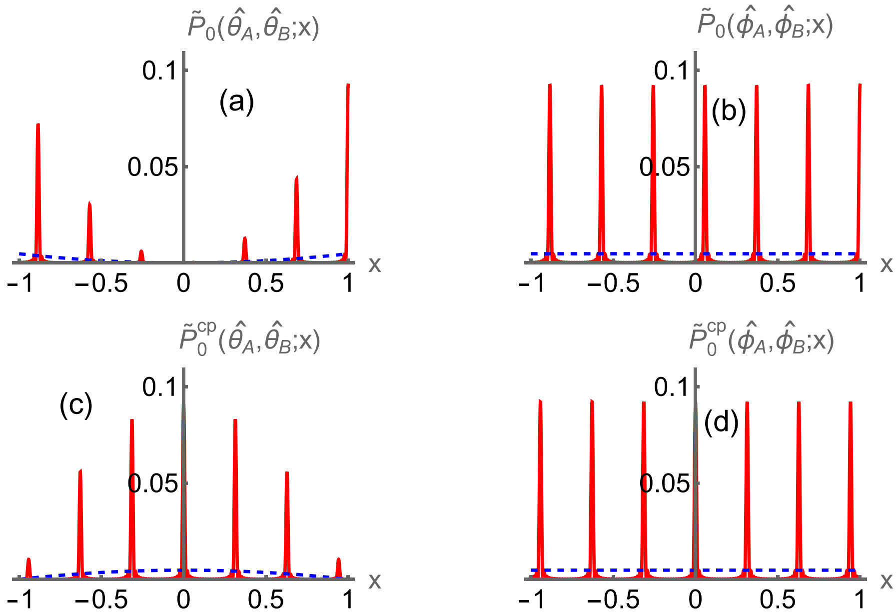

FIG. 7. Joint probability density $\tilde{P}_0(\boldsymbol{\alpha}_A, \boldsymbol{\alpha}_B; x)$ for copropagating excitation fields as a function of $x = \cos\theta_B$ for $\Omega_A = (0, 0)$, $\Omega_B = (\theta_B, 0)$, $\xi = 20$, $N = 20$, and $c_{3j}(0) = 1/\sqrt{20}$. (a) Copropagating, $(\boldsymbol{\alpha}_A, \boldsymbol{\alpha}_B) = (\hat{\boldsymbol{\theta}}_A, \hat{\boldsymbol{\theta}}_B)$; (b) copropagating, $(\boldsymbol{\alpha}_A, \boldsymbol{\alpha}_B) = (\hat{\boldsymbol{\phi}}_A, \hat{\boldsymbol{\phi}}_B)$; (c) counterpropagating, $(\boldsymbol{\alpha}_A, \boldsymbol{\alpha}_B) = (\hat{\boldsymbol{\theta}}_A, \hat{\boldsymbol{\theta}}_B)$; and (d) counterpropagating, $(\boldsymbol{\alpha}_A, \boldsymbol{\alpha}_B) = (\hat{\boldsymbol{\phi}}_A, \hat{\boldsymbol{\phi}}_B)$. The dashed curves are the single-atom result.

is taken to be a fully symmetric phased state, with $c_{j3}(0) = 1/\sqrt{N}$.

We restrict the discussion to the limit in which N and ξ are much greater than unity. If $\xi \gg 1$, the radiation emitted on the lower transition is approximately uniform and unpolarized. Moreover, the RE approximation can be expected to provide an excellent approximation to the exact results for the joint probability density. For this geometry, the RE approximation is

$$\tilde{P}_0(\boldsymbol{\alpha}_A, \boldsymbol{\alpha}_B; \Omega_A, \Omega_B) = \frac{3}{64N\pi^2 W(\Omega_A)} \Pi_{\boldsymbol{\alpha}_A,\boldsymbol{\alpha}_B}(\Omega_A, \Omega_B) F(k, \kappa, \Omega_A, \Omega_B), \quad (58)$$

where

$$F(k, \kappa, \Omega_A, \Omega_B) = \frac{\sin^2\left[\frac{Nkd}{2}(\cos\theta_A + \cos\theta_B - \kappa/k)\right]}{\sin^2\left[\frac{kd}{2}(\cos\theta_A + \cos\theta_B - \kappa/k)\right]}; \quad (59)$$

the $\Pi_{\boldsymbol{\alpha}_A,\boldsymbol{\alpha}_B}(\Omega_A, \Omega_B)$ are given in Eqs. (28) and $W(\Omega_A)$ by Eq. (53). If $\xi \gg 1$, $W(\Omega_A) \approx 1$.

1. Copropagating excitation fields

For copropagating excitation fields, we set $\kappa = 2k$ and $\Omega_A = (0, 0)$. In that limit

$$\tilde{P}_0(\hat{\boldsymbol{\theta}}_A, \hat{\boldsymbol{\theta}}_B; x) = \frac{3}{64N\pi^2 W(0)} \cos^2\theta_B \cos^2\phi_B F(\xi, x), \quad (60a)$$

$$\tilde{P}_0(\hat{\boldsymbol{\theta}}_A, \hat{\boldsymbol{\phi}}_B; x) = \frac{3}{64N\pi^2 W(0)} \sin^2\phi_B F(\xi, x), \quad (60b)$$

$$\tilde{P}_0(\hat{\boldsymbol{\phi}}_A, \hat{\boldsymbol{\theta}}_B; x) = \frac{3}{64N\pi^2 W(0)} \cos^2\theta_B \sin^2\phi_B F(\xi, x), \quad (60c)$$

$$\tilde{P}_0(\hat{\boldsymbol{\phi}}_A, \hat{\boldsymbol{\phi}}_B; x) = \frac{3}{64N\pi^2 W(0)} \cos^2\phi_B F(\xi, x), \quad (60d)$$

where

$$F(\xi, x) = \frac{\sin^2\left[\frac{N\xi}{2}(1-x)\right]}{\sin^2\left[\frac{\xi}{2}(1-x)\right]}, \quad (61)$$

and $x = \cos\theta_B$. The principal resonance occurs for $x = 1$ $(\theta_B = 0)$, and additional Bragg resonances when

$$x_q = 1 - \frac{2q\pi}{\xi}; \quad q = 1, 2....\mathrm{Int}\left(\frac{\xi}{\pi}\right),$$

where Int (y) is the integer part of y. In other words, there is a total of $[1 + \mathrm{Int}(\xi/\pi)]$ resonances. If N and ξ are much greater than unity, the resonances are resolved, since the width of each Bragg resonance is $\Delta x = 4\pi/N\xi$ (the width of the principal resonance is $2\pi/N\xi$) and adjacent resonances are separated by $x_{q+1} - x_q = 2\pi/\xi$.

In Figs. 7(a) and 7(b), $\tilde{P}_0(\hat{\boldsymbol{\theta}}_A, \hat{\boldsymbol{\theta}}_B; \Omega_A, \Omega_B)$ and $\tilde{P}_0(\hat{\boldsymbol{\phi}}_A, \hat{\boldsymbol{\phi}}_B; \Omega_A, \Omega_B)$ are plotted as a function of $x = \cos\theta_B$ for $\xi = 20$, $N = 20$, $W(0) = 1.03$, $\Omega_B = (\theta_B, 0)$, $\Omega_A = (0, 0)$, and $c_{3j}(0) = 1/\sqrt{20}$. The dashed curves in these figures are the corresponding single-atom results. The maximum ratio of the two probabilities at the resonance positions, $x = x_j$, is approximately equal to 20, as expected for maximum constructive interference. The fraction of the signal in the forward peak is 0.071. However, the fraction of the signal contained in all the resonances is 0.905 for $\tilde{P}_0(\hat{\boldsymbol{\phi}}_A, \hat{\boldsymbol{\phi}}_B)$ and 0.908 for $\tilde{P}_0(\hat{\boldsymbol{\theta}}_A, \hat{\boldsymbol{\theta}}_B)$, which are a general result when N and ξ are much greater than unity. In other words, although each resonance contains a fraction of the signal that is proportional to $1/\xi$, the total number of resonances scales with ξ, so that the fraction of the signal in *all* the resonance becomes independent of ξ for $\xi \gg 1$. Note that, even though the signal is confined to the phase-matched peaks, the emission is not temporally superradiant, $W(0) \approx 1$.

2. Counterpropagating excitation fields

For counterpropagating excitation fields, we set $\kappa = 0$ and $\Omega_A = (\pi/2, 0)$. In that limit,

$$\tilde{P}_0^{cp}(\hat{\boldsymbol{\theta}}_A, \hat{\boldsymbol{\theta}}_B; x) = \frac{3}{64N\pi^2 W(0)} \sin^2\theta_B F^{cp}(\xi, x), \tag{62a}$$

$$\tilde{P}_0^{cp}(\hat{\boldsymbol{\theta}}_A, \hat{\boldsymbol{\phi}}_B; x) = 0, \tag{62b}$$

$$\tilde{P}_0^{cp}(\hat{\boldsymbol{\phi}}_A, \hat{\boldsymbol{\theta}}_B; x) = \frac{3}{64N\pi^2 W(0)} \cos^2\theta_B \sin^2\phi_B F^{cp}(\xi, x), \tag{62c}$$

$$\tilde{P}_0^{cp}(\hat{\boldsymbol{\phi}}_A, \hat{\boldsymbol{\phi}}_B; x) = \frac{3}{64N\pi^2 W(0)} \cos^2\phi_B F^{cp}(\xi, x), \tag{62d}$$

where

$$F^{cp}(\xi, x) = \frac{\sin^2[N\xi x/2]}{\sin^2[\xi x/2]}. \tag{63}$$

There is the principal resonance when $x = 0$ ($\theta_B = \pi/2$) and additional Bragg resonances when

$$x_q = \pm\frac{2q\pi}{\xi}; \quad q = 1, 2....\mathrm{Int}\left(\frac{\xi}{2\pi}\right).$$

As for copropagating excitation fields, there is a total of $[1 + \mathrm{Int}(\xi/\pi)]$ resonances.

In Figs. 7(c) and 7(d), $\tilde{P}_0(\hat{\boldsymbol{\theta}}_A, \hat{\boldsymbol{\theta}}_B; \Omega_A, \Omega_B)$ and $\tilde{P}_0(\hat{\boldsymbol{\phi}}_A, \hat{\boldsymbol{\phi}}_B; \Omega_A, \Omega_B)$ are plotted as a function of x for $\Omega_A = (\pi/2, 0)$, $\xi = 20$, $N = 20$, $W(0) = 1.03$, $\Omega_A = (\pi/2, 0)$, $\Omega_B = (\theta_B, 0)$, and $c_{3j}(0) = 1/\sqrt{20}$. The dashed curves in these figures are the corresponding single-atom results. The maximum ratio of the two probabilities at the resonance positions, $x = x_j$, is approximately equal to 20, as expected for maximum constructive interference. The fraction of the signal contained in all the resonances is 0.975 for $\tilde{P}_0(\hat{\boldsymbol{\phi}}_A, \hat{\boldsymbol{\phi}}_B)$ and 0.908 for $\tilde{P}_0(\hat{\boldsymbol{\theta}}_A, \hat{\boldsymbol{\theta}}_B)$.

IV. DISCUSSION

We have studied cascade emission from an ensemble of N fixed atoms having a $J = 0 - 1 - 0$ level scheme. The atoms are prepared in a spatially phased superposition of their ground and upper states, and they share a single excitation. The time-integrated radiation pattern can be characterized by two distinct, but related, probability densities. First, there is the conditional joint probability density $P(\boldsymbol{\alpha}_A, \boldsymbol{\alpha}_B; \Omega_A, \Omega_B)$ that [a photon is emitted on the upper transition having polarization $\boldsymbol{\alpha}_A$ and direction $\hat{\mathbf{k}}_A = \Omega_A = (\theta_A, \phi_A)$] + [a photon is emitted on the lower transition having polarization $\boldsymbol{\alpha}_B$ and direction $\hat{\mathbf{k}}_B = \Omega_B = (\theta_B, \phi_B)$]. In addition, there are the individual probability densities $P_A(\hat{\boldsymbol{\alpha}}_A; \Omega_A)$ and $P_B(\hat{\boldsymbol{\alpha}}_B; \Omega_B)$ that a photon is emitted on the upper or lower transition, respectively, having polarization $\hat{\boldsymbol{\alpha}}$ and direction $\Omega_\alpha = (\theta_\alpha, \phi_\alpha)$. We have seen that the Rehler-Eberly approximation leads to good agreement with the exact results for the joint probability density, even if it can lead to unphysical results for the radiation patterns emitted on the upper and lower transitions separately.

The conditional joint probability density is characterized by two components. First, there is a contribution that corresponds to a superposition from individual atoms in which the emission on the upper and lower transitions originates from the *same* atoms. This contribution can be phase matched, with $P(\boldsymbol{\alpha}_A, \boldsymbol{\alpha}_B; \Omega_A, \Omega_B)$ proportional to N for the principal phase-matched signal. For copropagating excitation fields, the principal phase-matched signal occurs when the radiation on both transitions is emitted in the direction of the incident fields, even if k_{21} and k_{32} differ. In the case of counterpropagating excitation fields, the principal phase-matched signal occurs only if $k_{21} \approx k_{32}$ and $\hat{\mathbf{k}}_B \approx -\hat{\mathbf{k}}_A$ for a three-dimensional atomic ensemble. In contrast to the copropagating case, phase matching can occur for any direction of emission of the radiation on the upper transition. For the phase-matched emission to be optimal with either co- or counterpropagating excitation fields, the atoms must be prepared in a symmetric phased state. In addition to the principle phase-matched signals, there can be secondary phase-matched signals at angles for which the Bragg condition is satisfied. It should be noted that the phase-matched component, although arising from emission on the upper and lower transitions from the same atoms, is still affected by excitation exchange between the atoms.

The second contribution to the conditional joint probability density is a sum of terms in which radiation is emitted on the upper transition in one atom, taking that atom to its intermediate state, followed by a transfer of this intermediate state excitation to *another* atom via the dipole-dipole interaction which, in turn, radiates on the lower transition. This term is generally much smaller than the first contribution for interatomic separations that are much larger than a wavelength.

The radiation on the upper transition is isotropic and unpolarized, whereas the radiation on the lower transition can be polarized and anisotropic. However, the radiation on the lower transition becomes isotropic and unpolarized if $k_{21} \approx k_{32}$, $\hat{\mathbf{k}}_B \approx -\hat{\mathbf{k}}_A$, $\kappa = 0$, and $c_{3j}(0) = 1/\sqrt{N}$ (fully symmetric initial state). One can use angular momentum conservation to understand why the radiation on the lower transition must be isotropic *if* it is unpolarized. Initially, the atomic angular momentum of the atoms is equal to zero. Thus, the total angular momentum (spin plus orbital) of the radiated fields must also vanish. The emission on the upper transition is both isotropic and unpolarized—the angular momentum associated with this radiation vanishes. As a consequence, the angular momentum of the emission of the lower transition must also vanish. If the radiation is isotropic, it has zero orbital angular momentum, so it must also have zero spin angular momentum—it is unpolarized. When any of the conditions $k_{21} \approx k_{32}$, $\hat{\mathbf{k}}_B \approx -\hat{\mathbf{k}}_A$, $\kappa = 0$, and $c_{3j}(0) = 1/\sqrt{N}$ are violated, the overall symmetry is broken and the radiation emitted on the lower transition is both unpolarized and anisotropic in just the manner needed to ensure that the total angular momentum of the field vanishes.

Our results are applicable in settings involving cascade emission in atomic arrays, with potential applications in quantum information protocols. For example, we have shown that phase-matched emission into the largest possible solid angle, a desirable feature for a wave-vector-multiplexed protocol such as the one discussed in Ref. [15], is achieved using counterpropagating excitation fields on transitions having nearly equal frequencies (e.g., the 780–776-nm ladder scheme in rubidium). More generally, we have provided a framework that fully incorporates both the magnetic state substructure of the relevant transitions and the polarizations of the radiated fields.

ACKNOWLEDGMENTS

This research is supported by the Air Force Office of Scientific Research and the National Science Foundation.

APPENDIX A: VALUES OF $H^{\lambda}_{Am}(\Omega_A)$, $H^{\lambda}_{Bm}(\Omega_B)$, F_j, J_{α_A,α_B}, K_{α_A,α_B}, L_{α_A,α_B}, M_{α_A,α_B}, AND $G_{ij}(\mathbf{R})$

The values for $H^{\lambda}_{Am}(\Omega_A)$ and $H^{\lambda}_{Bm}(\Omega_B)$ are given by

$$H^{\theta}_{Am}(\Omega_A) = -\frac{e^{-i\phi_A}\cos\theta_A}{\sqrt{6}}\delta_{m,1} + \frac{e^{i\phi_A}\cos\theta_A}{\sqrt{6}}\delta_{m,-1} - \frac{\sin\theta_A}{\sqrt{3}}\delta_{m,0}, \tag{A1a}$$

$$H^{\phi}_{Am}(\Omega_A) = i\frac{e^{-i\phi_A}}{\sqrt{6}}\delta_{m,1} + i\frac{e^{i\phi_A}}{\sqrt{6}}\delta_{m,-1} + 0\delta_{m,0}, \tag{A1b}$$

$$H^{\theta}_{Bm}(\Omega_B) = \frac{e^{i\phi_B}\cos\theta_B}{\sqrt{6}}\delta_{m,1} - \frac{e^{-i\phi_B}\cos\theta_B}{\sqrt{6}}\delta_{m,-1} + \frac{\sin\theta_B}{\sqrt{3}}\delta_{m,0}, \tag{A1c}$$

$$H^{\phi}_{Bm}(\Omega_B) = i\frac{e^{i\phi_B}}{\sqrt{6}}\delta_{m,1} + i\frac{e^{-i\phi_B}}{\sqrt{6}}\delta_{m,-1} + 0\delta_{m,0}. \tag{A1d}$$

Note that

$$H^{\lambda}_{Bm}(\Omega_B) = -\left[H^{\lambda}_{Am}(\Omega_B)\right]^*.$$

The values of F, J, K, L, and M are given by [14]

$$F_1 = ([c_{13}(0)]^2 + [c_{31}(0)]^2) + 2c_{13}(0)c_{31}(0)\cos\left[(\kappa - k_{32}\cos\theta_A - k_{21}\cos\theta_B)Z_0\right], \tag{A2a}$$

$$F_2 = ([c_{13}(0)]^2 + [c_{31}(0)]^2) + 2c_{13}(0)c_{31}(0)\cos\left[(\kappa - k_{32}\cos\theta_A + k_{21}\cos\theta_B)Z_0\right], \tag{A2b}$$

$$F_3 = 2([c_{13}(0)]^2 + [c_{31}(0)]^2)\cos(k_{21}Z_0\cos\theta_B) + 4c_{13}(0)c_{31}(0)\cos(\kappa Z_0 - k_{32}Z_0\cos\theta_A), \tag{A2c}$$

$$F_4 = -2([c_{31}(0)]^2 - [c_{13}(0)]^2)\cos(k_{21}Z_0\cos\theta_B), \tag{A2d}$$

and

$$\begin{aligned} J_{\hat{\theta}_A,\hat{\theta}_B} =& \frac{\cos^2\theta_A\cos^2\theta_B\cos^2(\phi_A-\phi_B)}{\left(1-p_1^2\right)\left(1+q_1^2\right)}\left(2-p_1^2+q_1^2\right) \\ &+ \frac{\sin^2\theta_A\sin^2\theta_B}{\left(1-p_0^2\right)\left(1+q_0^2\right)}\left(2-p_0^2+q_0^2\right) \\ &+ 4\cos(\phi_A-\phi_B)\sin(2\theta_A)\sin(2\theta_B)\,\mathrm{Re}\left[\frac{4-(p_0+iq_0)^2-(p_1-iq_1)^2}{D}\right], \end{aligned} \tag{A3a}$$

$$\begin{aligned} K_{\hat{\theta}_A,\hat{\theta}_B} =& \left[\left(p_1^2+q_1^2\right)\frac{\cos^2\theta_A\cos^2\theta_B\cos^2(\phi_A-\phi_B)}{\left(1-p_1^2\right)\left(1+q_1^2\right)} + \left(p_0^2+q_0^2\right)\frac{\sin^2\theta_A\sin^2\theta_B}{\left(1-p_0^2\right)\left(1+q_0^2\right)}\right] \\ &+ 8\cos(\phi_A-\phi_B)\sin(2\theta_A)\sin(2\theta_B)\,\mathrm{Re}\left[\frac{(p_0+iq_0)(p_1-iq_1)}{D}\right], \end{aligned} \tag{A3b}$$

$$\begin{aligned} L_{\hat{\theta}_A,\hat{\theta}_B} =& -p_1\frac{\cos^2\theta_A\cos^2\theta_B\cos^2(\phi_A-\phi_B)}{1-p_1^2} - p_0\frac{\sin^2\theta_A\sin^2\theta_B}{1-p_0^2} \\ &+ \frac{(p_1+p_0)\left[-4+(p_1+p_0)^2+(q_1-q_0)^2\right]\cos(\phi_A-\phi_B)\sin(2\theta_A)\sin(2\theta_B)}{\left[(2+p_1+p_0)^2+(q_1-q_0)^2\right]\left[(2-p_1-p_0)^2+(q_1-q_0)^2\right]}, \end{aligned} \tag{A3c}$$

$$\begin{aligned} M_{\hat{\theta}_A,\hat{\theta}_B} =& q_1\frac{\cos^2\theta_A\cos^2\theta_B\cos^2(\phi_A-\phi_B)}{1+q_1^2} + q_0\frac{\sin^2\theta_A\sin^2\theta_B}{1+q_0^2} \\ &+ \frac{(q_1+q_0)\cos(\phi_A-\phi_B)\sin(2\theta_A)\sin(2\theta_B)}{2\left[(2-p_1+p_0)^2+(q_1+q_0)^2\right]\left[(2+p_1-p_0)^2+(q_1+q_0)^2\right]}, \end{aligned} \tag{A3d}$$

where

$$D = [-2 + p_1 + p_0 - i(q_1 - q_0)][2 + p_1 + p_0 - i(q_1 - q_0)] \times [2 - p_1 + p_0 + i(q_1 + q_0)][-2 - p_1 + p_0 + i(q_1 + q_0)]. \tag{A4}$$

For $\boldsymbol{\alpha}_A, \boldsymbol{\alpha}_B \neq \hat{\boldsymbol{\theta}}_A, \hat{\boldsymbol{\theta}}_B$

$$J_{\boldsymbol{\alpha}_A,\boldsymbol{\alpha}_B} = \frac{\left(2 - p_1^2 + q_1^2\right)}{\left(1 - p_1^2\right)\left(1 + q_1^2\right)} X_{\boldsymbol{\alpha}_A,\boldsymbol{\alpha}_B}; \quad K_{\boldsymbol{\alpha}_A,\boldsymbol{\alpha}_B} = \frac{\left(p_1^2 + q_1^2\right)}{\left(1 - p_1^2\right)\left(1 + q_1^2\right)} X_{\boldsymbol{\alpha}_A,\boldsymbol{\alpha}_B}, \tag{A5}$$

$$L_{\boldsymbol{\alpha}_A,\boldsymbol{\alpha}_B} = -\frac{p_1}{1 - p_1^2} X_{\boldsymbol{\alpha}_A,\boldsymbol{\alpha}_B}; \quad M_{\boldsymbol{\alpha}_A,\boldsymbol{\alpha}_B} = \frac{q_1}{1 + q_1^2} X_{\boldsymbol{\alpha}_A,\boldsymbol{\alpha}_B}, \tag{A6}$$

with

$$X_{\hat{\boldsymbol{\theta}}_A,\hat{\boldsymbol{\phi}}_B} = \cos^2\theta_A \sin^2(\phi_A - \phi_B), \tag{A7a}$$

$$X_{\hat{\boldsymbol{\phi}}_A,\hat{\boldsymbol{\theta}}_B} = \cos^2\theta_2 \sin^2(\phi_A - \phi_B), \tag{A7b}$$

$$X_{\hat{\boldsymbol{\phi}}_A,\hat{\boldsymbol{\phi}}_B} = \cos^2(\phi_A - \phi_B). \tag{A7c}$$

The values of the propagators $G_{mm'}(\mathbf{R})$ are given by

$$G_{11}(\mathbf{R}) = \sqrt{4\pi} h_0(k_B R) Y_{0,0}(\hat{\mathbf{R}}) - \frac{1}{2}\sqrt{\frac{4\pi}{5}} h_2(k_B R) Y_{2,0}(\hat{\mathbf{R}}), \tag{A8a}$$

$$G_{00}(\mathbf{R}) = \sqrt{4\pi} h_0(k_B R) Y_{0,0}(\hat{\mathbf{R}}) + \sqrt{\frac{4\pi}{5}} h_2(k_B R) Y_{2,0}(\hat{\mathbf{R}}), \tag{A8b}$$

$$G_{1,-1}(\mathbf{R}) = -\frac{3}{2}\sqrt{\frac{8\pi}{15}} h_2(k_B R) Y_{2,2}(\hat{\mathbf{R}}), \tag{A8c}$$

$$G_{-1,1}(\mathbf{R}) = -\frac{3}{2}\sqrt{\frac{8\pi}{15}} h_2(k_B R) Y_{2,-2}(\hat{\mathbf{R}}), \tag{A8d}$$

$$G_{1,0}(\mathbf{R}) = \frac{3}{2}\sqrt{\frac{4\pi}{15}} h_2(k_B R) Y_{2,1}(\hat{\mathbf{R}}), \tag{A8e}$$

$$G_{-1,0}(\mathbf{R}) = \frac{3}{2}\sqrt{\frac{4\pi}{15}} h_2(k_B R) Y_{2,-1}(\hat{\mathbf{R}}), \tag{A8f}$$

where h_ℓ is a spherical Hankel function and $Y_{\ell,m}(\hat{\mathbf{R}})$ is a spherical harmonic. The remaining $G_{m_j,m_s'}$s are obtained using $G_{-1,-1} = G_{11}$, $G_{0,-1} = -G_{1,0}$, and $G_{0,1} = -G_{-1,0}$. Note that $G_{mm'}(\mathbf{R}) = G_{mm'}(-\mathbf{R})$.

APPENDIX B: PERTURBATION SOLUTION

To explore how the emission on the lower transition is isotropic and unpolarized when $k_{21} = k_{32} = k$, $\kappa = 0$, $c_{j3}(0) = 1/\sqrt{N}$, we consider the limit in which all the interatomic separations are large, $\xi_{jj'} = kR_{jj'} \gg 1$ for $j \neq j'$. We set $\kappa = 0$, but for the moment do not set $k_{21} = k_{32}$, in order to show why this condition is necessary. We will obtain a solution for the $\hat{\boldsymbol{\phi}}_B$ component of the radiation on the lower transition to lowest order in $1/\xi_{jj'}$. An analogous calculation could be carried out for the $\hat{\boldsymbol{\theta}}$ component.

The $\hat{\boldsymbol{\phi}}$ component is given by

$$P_B(\hat{\boldsymbol{\phi}}_B, \Omega_B) = \frac{1}{8\pi} + \frac{27}{64N\pi^2} \sum_{m,m',\bar{m},\bar{m}'} \sum_{i,i',j,j'} \int d\Omega_A \begin{bmatrix} H(\hat{\boldsymbol{\theta}}_A, \hat{\boldsymbol{\phi}}_B, \Omega_A, \Omega_B, m, m', \bar{m}, \bar{m}') \\ +H(\hat{\boldsymbol{\phi}}_A, \hat{\boldsymbol{\phi}}_B, \Omega_A, \Omega_B, m, m', \bar{m}, \bar{m}') \end{bmatrix} \times V(im, jm'; i'\bar{m}, j'\bar{m}') e^{-ik_{21}\hat{\mathbf{k}}_B\cdot\mathbf{R}_{ii'}} e^{-ik_{32}\hat{\mathbf{k}}_A\cdot\mathbf{R}_{jj'}}. \tag{B1}$$

In the limit that $\xi_{jj'} \gg 1$, we can use Eqs. (B1) and (42) to obtain

$$\begin{aligned} V(im, jm'; i'\bar{m}, j'\bar{m}') &\approx [\delta_{i,j}\delta_{m,m'} - (1 - \delta_{i,j})G_{mm'}(k_{21}, R_{ij})/2][\delta_{i'j'}\delta_{\bar{m},\bar{m}'} - (1 - \delta_{i',j'})G^*_{\bar{m},\bar{m}'}(k_{21}, R_{i'j'})/2] \\ &\approx \delta_{i,j}\delta_{m,m'}\delta_{i'j'}\delta_{\bar{m},\bar{m}'} - \delta_{i'j'}\delta_{\bar{m},\bar{m}'}(1 - \delta_{i,j})G_{mm'}(k_{21}, R_{ij})/2 - \delta_{i,j}\delta_{m,m'}(1 - \delta_{i',j'})G^*_{\bar{m},\bar{m}'}(k_{21}, R_{i'j'})/2, \end{aligned} \tag{B2}$$

where the explicit dependence of G on k_{21} has been indicated. We expand

$$e^{-ik_{32}\hat{\mathbf{k}}_A\cdot\mathbf{R}_{jj'}} = 4\pi\sum_{\ell=0}^{\infty} i^{\ell}Y_{\ell m}(\Omega_A)Y^*_{\ell m}(-\hat{\mathbf{R}}_{jj'})j_{\ell}(k_{32}R_{jj'}), \tag{B3}$$

where j_ℓ is a spherical Bessel function. Keeping terms to lowest order in $1/\xi_{jj'}$, we then find

$$P_B(\hat{\boldsymbol{\phi}}_B,\Omega_B) \approx \frac{1}{8\pi} + \frac{27}{64N\pi^2}\sum_{m,m',\bar{m},\bar{m}'}\sum_{i,i',j,j'}\int d\Omega_A\begin{bmatrix}H(\hat{\boldsymbol{\theta}}_A,\hat{\boldsymbol{\phi}}_B,\Omega_A,\Omega_B,m,m',\bar{m},\bar{m}')\\ +H(\hat{\boldsymbol{\phi}}_A,\hat{\boldsymbol{\phi}}_B,\Omega_A,\Omega_B,m,m',\bar{m},\bar{m}')\end{bmatrix}e^{-ik_{21}\hat{\mathbf{k}}_B\cdot\mathbf{R}_{ii'}}e^{-ik_{32}\hat{\mathbf{k}}_A\cdot\mathbf{R}_{jj'}}$$
$$\times\{\delta_{i,j}\delta_{m,m'}\delta_{i'j'}\delta_{\bar{m},\bar{m}'} - \delta_{i'j'}\delta_{\bar{m},\bar{m}'}(1-\delta_{i,j})G_{mm'}(k_B,R_{ij})/2 - \delta_{i,j}\delta_{m,m'}(1-\delta_{i',j'})G^*_{\bar{m},\bar{m}'}(k_B,R_{i'j'})/2\}. \tag{B4}$$

In carrying out the integral over Ω_A, only terms with $\ell = 0$ and $\ell = 2$ contribute,

$$\begin{aligned}P_B(\hat{\boldsymbol{\phi}}_B,\Omega_B) \approx{}& \frac{1}{8\pi} + \frac{1}{8N\pi}\sum_{j,j'}(1-\delta_{j,j'})e^{-ik_{21}\hat{\mathbf{k}}_B\cdot\mathbf{R}_{ii'}}\left\{\begin{array}{c}j_0(k_{32}R_{jj'})\\ -\frac{3}{32}j_2(k_{32}R_{jj'})\sin^2\theta_{jj'}\cos[2(\phi_B-\phi_{jj'})]\\ -\frac{1}{27}j_2(k_{32}R_{jj'})[1+3\cos(2\theta_{jj'})]\end{array}\right\}\\ &-\frac{1}{16N\pi}\sum_{i,j}(1-\delta_{i,j})e^{-ik_{21}\hat{\mathbf{k}}_B\cdot\mathbf{R}_{ii'}}\left\{\begin{array}{c}h_0(k_{21}R_{ij})\\ -\frac{3}{32}h_2(k_{21}R_{ij})\sin^2\theta_{ij}\cos[2(\phi_B-\phi_{ij})]\\ -\frac{1}{27}h_2(k_{21}R_{ij})[1+3\cos(2\theta_{jj'})]\end{array}\right\}\\ &-\frac{1}{16N\pi}\sum_{i',j'}(1-\delta_{i',j'})e^{-ik_{21}\hat{\mathbf{k}}_B\cdot\mathbf{R}_{ii'}}\left\{\begin{array}{c}h_0^*(k_{21}R_{i',j'})\\ -\frac{3}{32}h_2^*(k_{21}R_{i'j'})\sin^2\theta_{i',j'}\cos[2(\phi_B-\phi_{i',j'})]\\ -\frac{1}{27}h_2^*(k_{21}R_{i'j'})[1+3\cos(2\theta_{jj'})]\end{array}\right\},\end{aligned} \tag{B5}$$

where $(\theta_{jj'},\phi_{jj'})$ are the spherical angle of $\hat{\mathbf{R}}_{jj'}$ and h_ℓ is a spherical Hankel function. If $k_{21} \neq k_{32}$, there is no cancellation of these terms. However, when $k_{21} = k_{32} = k$, the summation terms cancel and we find

$$P_B(\hat{\boldsymbol{\phi}}_B,\Omega_B) \approx \frac{1}{8\pi}. \tag{B6}$$

In going to higher order, we would find that terms varying as $G^{n-1}e^{-ik_{32}\hat{\mathbf{k}}_A\cdot\mathbf{R}_{jj'}}$ will be canceled by terms varying as $G^n e^{-ik_{32}\hat{\mathbf{k}}_A\cdot\mathbf{R}_{jj'}}\delta_{j,j'}$.

[1] S. Wehner, D. Elkouss, and R. Hanson, Quantum internet: A vision for the road ahead, Science **362**, 6412 (2018).

[2] Y. Lei, F. K. Asadi, T. Zhong, A. Kuzmich, C. Simon, and M. Hosseini, Quantum optical memory for entanglement distribution, Optica **10**, 1511 (2023).

[3] J. Dajczgewand, J.-L. Le Gouët, A. Louchet-Chauvet, and Th. Chanelière, Large efficiency at telecom wavelength for optical quantum memories, Opt. Lett. **39**, 2711 (2014).

[4] M. Falamarzi Askarani, M. Grimau Puigibert, T. Lutz, V. B. Verma, M. D. Shaw, S. W. Nam, N. Sinclair, D. Oblak, and W. Tittel, Storage and reemission of heralded telecommunication-wavelength photons using a crystal waveguide, Phys. Rev. Appl. **11**, 054056 (2019).

[5] J. Jin, E. Saglamyurek, M. Grimau Puigibert, V. Verma, F. Marsili, S. W. Nam, D. Oblak, and W. Tittel, Telecom-wavelength atomic quantum memory in optical fiber for heralded polarization qubits, Phys. Rev. Lett. **115**, 140501 (2015).

[6] T. Chanelière, D. N. Matsukevich, S. D. Jenkins, T. A. B. Kennedy, M. S. Chapman, and A. Kuzmich, Quantum telecommunication based on atomic cascade transitions, Phys. Rev. Lett. **96**, 093604 (2006).

[7] A. G. Radnaev, Y. O. Dudin, R. Zhao, H. H. Jen, S. D. Jenkins, A. Kuzmich, and T. A. B. Kennedy, A quantum memory with telecom wavelength conversion, Nat. Phys. **6**, 894 (2010).

[8] Y. O. Dudin, A. G. Radnaev, R. Zhao, J. Z. Blumoff, T. A. B. Kennedy, and A. Kuzmich, Entanglement of light-shift compensated atomic spin waves with telecom light, Phys. Rev. Lett. **105**, 260502 (2010).

[9] S. E. Thomas, S. Sagona-Stophel, Z. Schofield, I. A. Walmsley, and P. M. Ledingham, Single-photon-compatible telecommunications-band quantum memory in a hot atomic gas, Phys. Rev. Appl. **19**, L031005 (2023).

[10] R. T. Willis, F. E. Becerra, L. A. Orozco, and S. L. Rolston, Photon statistics and polarization correlations at telecommunications wavelengths from a warm atomic ensemble, Opt. Express **19**, 14632 (2011).

[11] P. R. Berman and A. Kuzmich, Source-field approach to phase-matched cascade correlated emission, Phys. Rev. A **108**, 063713 (2023).

[12] N. E. Rehler and J. H. Eberly, Superradiance, Phys. Rev. A **3**, 1735 (1971).

[13] Y. Miroshnychenko, U. V. Poulsen, and K. Mølmer, Directional emission of single photons from small atomic samples, Phys. Rev. A **87**, 023821 (2013).

[14] H. Fu and P. R. Berman, Microscopic theory of spontaneous decay in a dielectric, Phys. Rev. A **72**, 022104 (2005).

[15] M. Parniak, M. Dabrowski, M. Mazelanik, A. Leszczynski, M. Lipka and W. Wasilewski, Wavevector multiplexed atomic quantum memory via spatially-resolved single-photon detection, Nat. Commun. **8**, 2140 (2017).